Nečas Center for Mathematical Modeling

hp-DGFEM for nonlinear convection-diffusion problems

V. Dolejší

Preprint no. 2013-0010

http://ncmm.karlin.mff.cuni.cz/

hp-DGFEM for nonlinear convection-diffusion problems ☆

Vít Dolejší[1]

Abstract

We deal with a numerical solution of nonlinear convection-diffusion problems with the aid of the discontinuous Galerkin finite element method (DGFEM). We propose a new *hp*-adaptation technique, which is based on a combination of a residuum-nonconformity estimator and a regularity indicator. The residuum-nonconformity estimator consists of two building blocks and it marks mesh elements for a refinement. The regularity indicator decides if the marked elements will be refined by *h*- or *p*-technique. The residuum-nonconformity estimator as well as the regularity indicator are easily computable quantities. Moreover, the same technique estimates an algebraic error arising from an iterative solution of the corresponding nonlinear algebraic system. The performance of the proposed *hp*-DGFEM is demonstrated by five numerical examples.

Keywords: *hp*-discontinuous Galerkin finite element method, residuum-nonconformity indicator, regularity estimator, algebraic error
2000 MSC: 65N30, 65N50, 65N22

1. Introduction

Our aim is to develop a sufficiently robust, efficient and accurate numerical scheme for the simulation of viscous compressible flows. The *discontinuous Galerkin* (DG) methods have become very popular numerical techniques for the solution of the compressible Navier-Stokes equations. DG space discretization uses (high order) piecewise polynomial discontinuous approximation on arbitrary meshes. DG methods were employed in many papers for the discretization of compressible fluid flow problems, see, e.g., [5, 6, 13, 15, 26–28, 30, 36] and the references cited therein. Recent progress of the use of the DG method for compressible flow simulations can be found in [38].

In this paper, we solve a scalar nonlinear convection-diffusion equation (which represents a model problem for the system of the compressible Navier-Stokes equations) with the aid of the DG method. We propose a new *hp*-adaptive method which allows the refinement in the element size h as well as in the polynomial degree p. Similarly as the h version of the finite element methods, a posteriori error estimates can be used to determine which elements should be refined. However, a single error estimate cannot simultaneously determine whether it is better to do h or p refinement. Several strategies for making this determination have been proposed over the years, see, e.g., [33] or [24] for a survey. Based on many theoretical works, e.g., monographs [43, 44] or papers [4, 11, 45] we expect that an error converges at an exponential rate in the number of degrees of freedom.

There exist many theoretical works deriving a posteriori error estimates based on various approaches for linear or quasi-linear problems. On the other hand, the amount of papers dealing with a posteriori error estimates for strongly non-linear problems is significantly smaller. Some overview of a posteriori error estimates can be found in [46]. An prototypical example for a nonlinear problem is the p-Laplacian operator analysed in several papers. However, with a few exceptions, e.g., [8], the error upper bounds involve unknown generic constants. In several works, e.g., [1, 7, 9, 16], a *residual flux-based dual norm* was used as an error measure. This approach allows to derive guaranteed bounds on the error, that is, error upper bounds without undetermined constants, and at the same

☆ This work is a part of the research project Grant No. 201/08/0012 of the Czech Science Foundation.
Email address: dolejsi@karlin.mff.cuni.cz (Vít Dolejší)
[1] Charles University Prague, Faculty of Mathematics and Physics, Sokolovská 83, 186 75 Praha, Czech Republic

time ensure robustness, that is, two-sided error bounds whose ratio is independent of the nonlinearity. A measurement of the error in a dual norm is a base of our approach presented here.

The aim of this paper is not to derive any guaranteed and robust a posteriori error estimate, but to develop an *hp*-algorithm which adaptively generates a "good" *hp*-mesh (mesh elements with the corresponding degrees of polynomial approximation). On this mesh, we compute a sufficiently accurate approximation of the exact solution with low computational costs. Although, we do not have a guaranteed error estimate, the presented numerical experiments show that our estimate gives reasonable information about an error.

The proposed *hp*-adaptation strategy is based on a combination of a residuum-nonconformity estimator and a regularity indicator. The *residuum-nonconformity estimator* gives a lower estimate of the error measure consisting of the error measured in a dual norm and the quantity measuring a violation of the conformity of the solution. This estimator is locally defined for each mesh element, it is easily computable and its implementation is very simple. The *regularity indicator* is based on the integration of interelement jumps of the approximate solution over the element boundary. Taking into account results from a priori error analysis (e.g., [14]), we define the regularity indicator. If this value is smaller than a priori known value (without any undetermined constant) then we apply *p*-refinement otherwise we use *h*-refinement. Both refinements (*h* and *p*) are only isotropic, anisotropic adaptation will be a subject of further research.

The content of the rest of the paper is the following. In Section 2, we present the convection-diffusion problem and recall its discontinuous Galerkin finite element (DGFE) discretization which leads to a nonlinear algebraic system. Its solution by an iterative method is described in Section 3. Furthermore, Section 4 introduces the approach of the residual dual norm as an error measure. Moreover, global, element and algebraic residuum estimators are defined. The resulting *hp*-DGFEM is presented in Section 5. A computational verification of the presented method for a scalar nonlinear convection-diffusion equation is given in Section 6. Finally, several concluding remarks are given in Section 7.

2. Problem description

2.1. Governing equations

We consider the nonlinear *convection-diffusion problem*

$$\nabla \cdot \boldsymbol{f}(u) - \nabla \cdot (\boldsymbol{K}(u)\nabla u) = g(x), \tag{1a}$$

$$u\big|_{\partial\Omega_D} = u_D, \tag{1b}$$

$$\boldsymbol{K}(u)\frac{\partial u}{\partial \boldsymbol{n}}\Big|_{\partial\Omega_N} = g_N, \tag{1c}$$

where $u : \Omega \to \mathbb{R}$ is the unknown scalar function defined on $\Omega \in \mathbb{R}^d$, $d = 2, 3$, we assume that Ω is polygonal for simplicity. Moreover, $\boldsymbol{f}(u) = (f_1(u), \dots, f_d(u)) : \mathbb{R} \to \mathbb{R}^d$ and $\boldsymbol{K}(u) = \{K_{ij}(u)\}_{i,j=1}^d : \mathbb{R} \to \mathbb{R}^{d\times d}$ are nonlinear functions of their arguments, $\boldsymbol{n}$ is the unit outer normal to $\partial\Omega$ and $\emptyset \neq \partial\Omega_D \cup \partial\Omega_N = \partial\Omega$ are disjoint parts of the boundary of Ω. Symbols ∇ and $\nabla\cdot$ mean the gradient and divergence operators, respectively.

We assume that $f_s \in C^1(\mathbb{R})$, $f_s(0) = 0$, $s = 1, \dots, d$, $\boldsymbol{K}$ is bounded and positively definite, $g \in L^2(\Omega)$, u_D is the trace of some $u^* \in H^1(\Omega) \cap L^\infty(\Omega)$ on $\partial\Omega_D$ and $g_N \in L^2(\partial\Omega_N)$. We use the standard notation for function spaces (see, e. g., [40]): $L^p(\Omega)$ denote the Lebesgue spaces and $W^{k,p}(\Omega)$, $H^k(\Omega) = W^{k,2}(\Omega)$ are the Sobolev spaces.

In order to introduce a weak solution, we define the spaces

$$V := \{v;\ v \in H^1(\Omega),\ v|_{\partial\Omega_D} = 0\}, \quad W := \{v;\ v \in H^1(\Omega),\ v - u^* \in V\}. \tag{2}$$

Definition 2.1. *We say that function u is the* weak solution *of (1), if the following conditions are satisfied*

$$\textit{a)} \qquad u \in W \cap L^\infty(\Omega), \tag{3a}$$

$$\textit{b)} \qquad \int_\Omega \left[\nabla \cdot \boldsymbol{f}(u)\, v + (\boldsymbol{K}(u)\nabla u) \cdot \nabla v\right] \mathrm{d}x = \int_\Omega g v \,\mathrm{d}x + \int_{\partial\Omega_N} u\, v \,\mathrm{d}S \qquad \forall v \in V. \tag{3b}$$

Let us note that the assumption $u \in L^\infty(\Omega)$ in (3a) guarantees the boundedness of functions $\boldsymbol{f}(u)$ and $\boldsymbol{K}(u)$ and therefore the existence of the integrals in (3b). This assumption can be weakened if functions $\boldsymbol{f}(u)$ and $\boldsymbol{K}(u)$ satisfy some growth conditions.

2.2. Discretization of the problem

2.2.1. Triangulations

Let $\mathscr{T}_h$ ($h > 0$) be a partition of the closure $\overline{\Omega}$ of the domain Ω into a finite number of closed d-dimensional simplicies K with mutually disjoint interiors. We call $\mathscr{T}_h = \{K\}_{K\in\mathscr{T}_h}$ a *triangulation* of Ω and do not require the conforming properties from the finite element method.

By $\mathscr{F}_h$ we denote the set of all open $(d-1)$-dimensional faces (open edges when $d = 2$ or open faces when $d = 3$) of all elements $K \in \mathscr{T}_h$. Further, the symbol $\mathscr{F}_h^I$ stands for the set of all $\Gamma \in \mathscr{F}_h$ that are contained in Ω (inner faces). Moreover, we introduce notations $\mathscr{F}_h^D$ and $\mathscr{F}_h^N$ for the sets of all $\Gamma \in \mathscr{F}_h$ such that $\Gamma \subset \partial\Omega_D$ and $\Gamma \subset \partial\Omega_N$, respectively. In order to simplify the notation, we put $\mathscr{F}_h^{ID} = \mathscr{F}_h^I \cup \mathscr{F}_h^D$ and $\mathscr{F}_h^B = \mathscr{F}_h^D \cup \mathscr{F}_h^N$ (superscript ^{B} as boundary). Finally, for each $\Gamma \in \mathscr{F}_h$, we define a unit normal vector $\boldsymbol{n}_\Gamma$. We assume that for $\Gamma \in \mathscr{F}_h^B$ the vector $\boldsymbol{n}_\Gamma$ has the same orientation as the outer normal of $\partial\Omega$. For $\boldsymbol{n}_\Gamma$, $\Gamma \in \mathscr{F}_h^I$, the orientation is arbitrary but fixed for each face.

2.2.2. Functional spaces

Over the triangulation $\mathscr{T}_h$ we define the so-called *broken Sobolev space* $H^s(\Omega, \mathscr{T}_h) := \{v; v|_K \in H^s(K)\ \forall K \in \mathscr{T}_h\}$, $s \geq 0$ with the seminorm $|v|_{H^s(\Omega,\mathscr{T}_h)} := \left(\sum_{K\in\mathscr{T}_h} |v|^2_{H^s(K)}\right)^{1/2}$, where $|\cdot|_{H^s(K)}$ denotes the seminorm of the Sobolev space $H^s(K)$, $K \in \mathscr{T}_h$.

Moreover, to each $K \in \mathscr{T}_h$, we assign a positive integer p_K (=local polynomial degree). Then we define the set $\mathsf{p}_h := \{p_K, K \in \mathscr{T}_h\}$ and the finite dimensional subspace of $H^1(\Omega, \mathscr{T}_h)$ which consists of discontinuous piecewise polynomial functions associated with the vector p_h by

$$S_{h\mathsf{p}} = \{v;\ v \in L^2(\Omega),\ v|_K \in P_{p_K}(K)\ \forall K \in \mathscr{T}_h\}, \tag{4}$$

where $P_{p_K}(K)$ denotes the space of all polynomials on K of degree $\leq p_K$, $K \in \mathscr{T}_h$.

Furthermore, for each $\Gamma \in \mathscr{F}_h^I$ there exist two elements $K^{(+)}, K^{(-)} \in \mathscr{T}_h$ such that $\Gamma \subset K^{(+)} \cap K^{(-)}$. We use the convention that $K^{(-)}$ lies in the direction of $\boldsymbol{n}_\Gamma$ and $K^{(+)}$ in the opposite direction of $\boldsymbol{n}_\Gamma$. Then for $v \in S_{h\mathsf{p}}$, we introduce the notation: $v|_\Gamma^{(+)}$ is the trace of $v|_{K^{(+)}}$ on Γ, $v|_\Gamma^{(-)}$ is the trace of $v|_{K^{(-)}}$ on Γ, $\{\{v\}\}_\Gamma := \left(v|_\Gamma^{(+)} + v|_\Gamma^{(-)}\right)/2$ denotes the mean value of v on Γ and $[\![v]\!]_\Gamma := v|_\Gamma^{(+)} - v|_\Gamma^{(-)}$ denotes the jump of v on Γ. Finally, for $\Gamma \in \mathscr{F}_h^B$, we denote by $v|_\Gamma^{(+)}$ the trace of $v|_{K^{(+)}}$ on Γ, where $K^{(+)} \in \mathscr{T}_h$ such that $\Gamma \subset K^{(+)} \cap \partial\Omega$, and we put $\{\{v\}\}_\Gamma = [\![v]\!]_\Gamma := v|_\Gamma^{(+)}$.

In case that $\boldsymbol{n}_\Gamma$, $[\![\cdot]\!]_\Gamma$ and $\{\{\cdot\}\}_\Gamma$ are arguments of $\int_\Gamma \ldots \mathrm{d}S$, $\Gamma \in \mathscr{F}_h$, we omit the subscript Γ and write simply $\boldsymbol{n}$, $[\![\cdot]\!]$ and $\{\{\cdot\}\}$, respectively.

2.2.3. DG discretization

We discretize equation (1a) with the aid of the interior penalty Galerkin (IPG) variant of the DGFE method in the same way as in [18, 39]. For $u, v \in H^2(\Omega, \mathscr{T}_h)$ we define the forms

$$\begin{aligned}\tilde{a}_h(u,v) \quad := \quad & \sum_{K\in\mathscr{T}_h}\int_K \boldsymbol{K}(u)\nabla u\cdot\nabla v\,\mathrm{d}x - \sum_{\Gamma\in\mathscr{F}_h^{ID}}\int_\Gamma \Big(\{\{\boldsymbol{K}(u)\nabla u\}\}\cdot\boldsymbol{n}[\![v]\!] - \mathrm{g}\{\{\boldsymbol{K}(u)\nabla v\}\}\cdot\boldsymbol{n}[\![u]\!]\Big)\,\mathrm{d}S \\ & + \sum_{\Gamma\in\mathscr{F}_h^{ID}}\int_\Gamma \sigma[\![u]\!]\,[\![v]\!]\,\mathrm{d}S + \sum_{\Gamma\in\mathscr{F}_h}\int_\Gamma H(u|_\Gamma^{(+)}, u|_\Gamma^{(-)}, \boldsymbol{n})\,[\![v]\!]\,\mathrm{d}S - \sum_{K\in\mathscr{T}_h}\int_K \boldsymbol{f}(u)\cdot\nabla v\,\mathrm{d}x,\end{aligned} \tag{5a}$$

$$\ell_h(u,v) \quad := \quad (g,v) + (g_N,v)_N + \int_{\partial\Omega_D}(\mathrm{g}\boldsymbol{K}(u)\nabla v\cdot\boldsymbol{n}\,u_D + \sigma v\,u_D)\,\mathrm{d}S, \tag{5b}$$

where $\mathrm{g} = -1, 0$ and 1 for SIPG, IIPG and NIPG variants of DGFE method, respectively, the penalty parameter σ is chosen by $\sigma|_\Gamma = \varepsilon C_W h_\Gamma^{-1}$, $\Gamma \in \mathscr{F}_h$, where $h_\Gamma = \mathrm{diam}(\Gamma)$, $\Gamma \in \mathscr{F}_h$, ε denotes the amount of diffusivity ($\approx \boldsymbol{K}(\cdot)$) and $C_W > 0$ is a suitable constant which guarantees the convergence of the method. The function H in (5a) is the *numerical flux*, well-known from finite volume methods (see, e.g., [25], Section 3.2), which approximates convective flux by $\boldsymbol{f}(u)\cdot\boldsymbol{n} \approx H\left(u|_\Gamma^{(+)}, u|_\Gamma^{(-)}, \boldsymbol{n}\right)$ on an element face. On $\partial\Omega_D$ the value $u|_\Gamma^{(-)}$ is taken from the boundary conditions (1b) and on $\partial\Omega_N$ the value $u|_\Gamma^{(-)}$ is extrapolated from the interior of Ω. We shall assume that the numerical flux is *conservative* and *consistent*, i.e., $H(u,v,\boldsymbol{n}) = -H(v,u,-\boldsymbol{n})$ and $H(u,u,\boldsymbol{n}) = \boldsymbol{f}(u)\cdot\boldsymbol{n}$, respectively, see [18] for details.

Furthermore, we put

$$\tilde{c}_h(u,v) := \tilde{a}_h(u,v) - \ell_h(u,v), \qquad u,v \in H^2(\Omega,\mathscr{T}_h), \tag{6}$$

Now, we are ready to define the discrete problem.

Definition 2.2. *We say that function $u_h \in S_{hp}$ is an* approximate solution *of (3), if*

$$\tilde{c}_h(u_h,v_h) = 0 \qquad \forall v_h \in S_{hp}. \tag{7}$$

Moreover, for the purpose of the error measure introduced in Section 4, we define the form $\mathcal{N}_h : H^1(\Omega,\mathscr{T}_h) \to \mathbb{R}$ by

$$\mathcal{N}_h(v) := \left(2 \sum_{\Gamma\in\mathscr{F}_h^I} \int_\Gamma h_\Gamma^{-1} [\![v]\!]^2 \,\mathrm{d}S + \sum_{\Gamma\in\mathscr{F}_h^D} \int_\Gamma h_\Gamma^{-1} (v-u_D)^2 \,\mathrm{d}S \right)^{1/2}, \tag{8}$$

where u_D is from (1b) and $h_\Gamma = \mathrm{diam}(\Gamma)$, $\Gamma \in \mathscr{F}_h$. We put the scaling factor 2 in front of the first due to the favorable property (38). Finally, we characterise the solution of (3).

Lemma 2.3. *The following implications are valid:*

i) Let $u \in H^2(\Omega)$ be the solution of (3) *then*

$$\tilde{c}_h(u,v_h) = 0 \quad \forall v_h \in H^2(\Omega,\mathscr{T}_h), \tag{9a}$$

$$\mathcal{N}_h(u) = 0. \tag{9b}$$

ii) If $u \in H^2(\Omega,\mathscr{T}_h)$ satisfies both conditions of (9) *then u is the solution of* (3)*.*

Proof. The assertion i) follows immediately from the the consistency of $\tilde{c}_h$, the continuity of traces of u on $\Gamma \in \mathscr{F}_h^I$ and the fact that $u = u_D$ on $\Gamma \in \mathscr{F}_h^D$. In order to prove ii) we observe that (9b) implies $u \in W$. Furthermore, identity (9a) for $u \in H^2(\Omega,\mathscr{T}_h) \cap W$ and $v \in H^1(\Omega)$ together with (3a), (5), (6) and the consistency of the numerical flux reads $0 = \tilde{c}_h(u,v) = \tilde{a}_h(u,v) - \ell_h(u,v)$ $\forall v \in V$ which proves that u is the solution of (3). □

3. Solution strategy

The discrete problem (7) represents a system of $N_h = \dim S_{hp}$ nonlinear algebraic equations. We solve it with the aid of a Newton-like iterative method. In our approach, we employ some ideas presented in [15, 19, 21], where the semi-implicit time discretization method for the solution of compressible flow problems was presented.

3.1. Linearization

In order to employ this approach, we assume that the numerical flux can be written in the form

$$H(u_1,u_2,\boldsymbol{n}) := P^+(u_1,u_2,\boldsymbol{n})u_1 + P^-(u_1,u_2,\boldsymbol{n})u_2, \tag{10}$$

where P^+ and P^- are suitable functions of their arguments. For example, the numerical fluxes based on the idea of *upwinding* can be written in the form (10), see [25].

Moreover, we introduce functions $A_s : \mathbb{R} \to \mathbb{R}$, $s = 1,\dots,d$ such that

$$f_s(u) \approx A_s(u)u, \quad u \in \mathbb{R},\ s = 1,\dots,d. \tag{11}$$

In this paper, we put $A_s(u) := f_s'(u)$, $u \in \mathbb{R}$, $s = 1,\dots,d$, which leads to the first order approximation of (11).

Finally, for $u,v,w \in H^2(\Omega,\mathscr{T}_h)$, we define the form

$$\begin{aligned} c_h(v,u,w) := {} & \sum_{K\in\mathscr{T}_h} \int_K \boldsymbol{K}(v)\nabla u\cdot\nabla w \,\mathrm{d}x - \sum_{\Gamma\in\mathscr{F}_h^{ID}} \int_\Gamma \Big(\{\!\{\boldsymbol{K}(v)\nabla u\}\!\}\cdot\boldsymbol{n}[\![w]\!] - \mathrm{g}\{\!\{\boldsymbol{K}(v)\nabla w\}\!\}\cdot\boldsymbol{n}[\![u]\!] \Big) \mathrm{d}S + J_h^\sigma(u,w) \\ & + \sum_{\Gamma\in\mathscr{F}_h} \int_\Gamma \left(P^+(v|_\Gamma^{(+)}, v|_\Gamma^{(-)}, \boldsymbol{n})u|_\Gamma^{(+)} + P^-(v|_\Gamma^{(+)}, v|_\Gamma^{(-)}, \boldsymbol{n})u|_\Gamma^{(-)} \right) [\![w]\!] \,\mathrm{d}S - \sum_{K\in\mathscr{T}_h} \int_K \sum_{s=1}^d A_s(v)u \frac{\partial w}{\partial x_s} \,\mathrm{d}x. \end{aligned} \tag{12}$$

The form c_h is nonlinear with respect to its first argument but linear with respect its second and third arguments. Moreover, due to (5a) – (5b), (10), (11) and (12), we have

$$c_h(u,u,v) - \ell_h(u,v) \approx \tilde{c}_h(u,v) \qquad \forall u,v \in H^2(\Omega,\mathscr{T}_h). \tag{13}$$

3.2. Algebraic representation

Let $\{\varphi_i(x),\ i = 1,\dots,N_h\}$ be a basis of $S_{h\mathsf{p}}$ which is constructed as a composition of local bases constructed separately for each $K \in \mathscr{T}_h$. See [21], where one possibility is described in details. Thus, each $u_h \in S_{h\mathsf{p}}$ can be expressed as

$$u_h(x) = \sum_{j=1}^{N_h} u^j \varphi_j(x), \qquad \boldsymbol{U}_h := \{u^j\}_{j=1}^{N_h} \in \mathbb{R}^{N_h}, \tag{14}$$

where $u^j \in \mathbb{R},\ j = 1,\dots,N_h$ are the basis coefficients. Obviously, (14) defines an isomorphism between $u_h \in S_{h\mathsf{p}}$ and $\boldsymbol{U}_h \in \mathbb{R}^{N_h}$. In order to rewrite the discrete problem (7), we define the vector-valued function

$$\boldsymbol{F}_h : \mathbb{R}^{N_h} \to \mathbb{R}^{N_h}, \quad \boldsymbol{F}_h(\boldsymbol{U}_h) := \{\tilde{c}_h(u_h,\varphi_i)\}_{i=1}^{N_h}. \tag{15}$$

Therefore, the discrete problem (7) reads

$$\text{find } \boldsymbol{U}_h \in \mathbb{R}^{N_h} \text{ such that } \boldsymbol{F}_h(\boldsymbol{U}_h) = \boldsymbol{0}. \tag{16}$$

3.3. Iterative method

To determine solution $\boldsymbol{U}_h$ of the system (16), we employ a damped Newton-like method which generates a sequence of approximations $\boldsymbol{U}_h^n,\ n = 0,1,\dots$ to the actual numerical solution $\boldsymbol{U}_h$ using the following algorithm. Given an iterate $\boldsymbol{U}_h^n$, the update $\boldsymbol{d}^n$ of $\boldsymbol{U}_h^n$ to get to the next iterate

$$\boldsymbol{U}_h^{n+1} := \boldsymbol{U}_h^n + \lambda^n \boldsymbol{d}^n \tag{17}$$

is defined by: find $\boldsymbol{d}^n \in \mathbb{R}^{N_h}$ such that

$$\mathbb{C}_h(\boldsymbol{U}_h^n)\boldsymbol{d}^n = -\boldsymbol{F}_h(\boldsymbol{U}_h^n), \tag{18}$$

where $\mathbb{C}_h$ is the *flux matrix* given by

$$\mathbb{C}_h(\boldsymbol{U}_h) := \left\{c_h\left(u_h,\varphi_j,\varphi_i\right)\right\}_{i,j=1}^{N_h}.$$

Obviously, due to the local character of basis functions, matrix $\mathbb{C}_h$ has a sparse block structure, see [21]. Moreover, $\lambda^n \in (0,1]$ is a damping parameter which ensures convergence of (17) – (18) in case when the initial guess $\boldsymbol{U}_h^0$ is far from the solution of (16).

Remark 3.1. *Let us note that in virtue of* (13)*, we have*

$$\boldsymbol{F}_h(\boldsymbol{U}_h) \approx \mathbb{C}_h(\boldsymbol{U}_h)\boldsymbol{U}_h - \boldsymbol{q}_h(\boldsymbol{U}_h) \qquad \forall \boldsymbol{U}_h \in \mathbb{R}^{N_h}, \tag{19}$$

where $\boldsymbol{q}_h(\boldsymbol{U}_h) \in \mathbb{R}^{N_h}$ corresponds to form ℓ_h by $\boldsymbol{q}_h(\boldsymbol{U}_h) = \{\ell_h(u_h,\varphi_i)\}_{i=1}^{N_h}$. The algorithm (17) – (18) *is the standard damped Newton method (see [12, Chapter 3]) with the approximation of the Jacobian by*

$$\frac{D\boldsymbol{F}_h(\boldsymbol{U}_h)}{D\boldsymbol{U}_h} \approx \mathbb{C}_h(\boldsymbol{U}_h), \tag{20}$$

which follows from (19) *if we omit derivatives of $\mathbb{C}_h$ and $\boldsymbol{q}_h$ with respect to their arguments.*

Remark 3.2. *In practice, it is not necessary to update the flux matrix $\mathbb{C}_h(\boldsymbol{U}_h^n)$ at each Newton iteration $n = 1,2,\dots$. Hence, in many cases, we replace* (18) *by*

$$\mathbb{C}_h(\boldsymbol{U}_h^0)\boldsymbol{d}^n = -\boldsymbol{F}_h(\boldsymbol{U}_h^n). \tag{21}$$

Concerning the choice of the damping parameter, we start from the value $\lambda^n = 1$ and evaluate a monitoring function $\theta^n := \left\|\boldsymbol{F}_h(\boldsymbol{U}_h^{n+1})\right\| / \left\|\boldsymbol{F}_h(\boldsymbol{U}_h^n)\right\|$. If $\theta^n < 1$ we proceed to the next Newton iteration. Otherwise, we put $\lambda^n := \lambda^n/2$ and repeat the actual Newton iteration. Analysis of the convergence of this simplified Newton method and the monitoring function can be found in [12].

The iterative process (17) – (18) is terminated if a suitable *algebraic stopping criterion* is achieved. In Section 4.3, we present an algebraic stopping criterion following from the framework of residuum estimators. Let $\tilde{\boldsymbol{U}}_h := \boldsymbol{U}_h^n$ denote the output of the iterative process (17) – (18), i.e., an approximation of $\boldsymbol{U}_h$ satisfying the stopping criterion. We denote by $\tilde{u}_h \in S_{h\mathsf{p}}$ the function corresponding to $\tilde{\boldsymbol{U}}_h$ by isomorphism (14). In general, $\tilde{u}_h$ does not satisfy the discrete problem (7) ($\tilde{c}_h(\tilde{u}_h, v_h) \neq 0,\ v_h \in S_{h\mathsf{p}}$), since it suffers from a (nonlinear) *algebraic error*.

Remark 3.3. *The linear algebraic system* (18) *is solved iteratively with the aid of GMRES method with a block ILU(0) preconditioning, see [21].*

4. Residuum estimator

In this section we investigate the discretization error $u - u_h$ and the algebraic error $\tilde{u}_h - u_h$ in a suitable (dual) norm and define estimators giving some information about these errors. Based on them we define the stopping criterion for the iterative process (17) – (18) and particularly, in Section 5, we propose the *hp*-adaptation strategy.

4.1. Error measure

Similarly as in [16], our proposed error measure consists of *two building blocks*, which are motivated by Lemma 2.3, namely relations (9a) and (9b). First, we proceed to a functional representation of the DG method. Let X be a linear function space such that $u \in X$ and $u_h \in X$. It is equipped with a norm $\|\cdot\|_X$. (The space X does not need to be complete with respect to $\|\cdot\|_X$.) In our case, $X := H^2(\Omega, \mathscr{T}_h)$, the norm $\|\cdot\|_X$ will be specified later. Let X' denote the dual space to X. Moreover, let $A_h : X \to X'$ be the nonlinear operator corresponding to $\tilde{c}_h$ by

$$\langle A_h u, v\rangle := \tilde{c}_h(u, v), \qquad u, v \in X, \tag{22}$$

where $\langle\cdot,\cdot\rangle$ denotes the duality between X' and X. We define the dual norm by

$$\|A_h u\|_{X'} := \sup_{0\neq v\in X} \frac{\langle A_h u, v\rangle}{\|v\|_X}. \tag{23}$$

In order to present the *first building block* we observe that if $u \in H^2(\Omega) \subset X$ is the solution of (3) then due to (9a) and (22), we have $A_h u = 0$. Then, the value

$$\mathcal{R}_h(u_h) := \|A_h u_h - A_h u\|_{X'} = \|A_h u_h\|_{X'} = \sup_{0\neq v\in X} \frac{\langle A_h u_h, v\rangle}{\|v\|_X} = \sup_{0\neq v\in X} \frac{\tilde{c}_h(u_h, v)}{\|v\|_X} \tag{24}$$

defines the *residuum error in the dual norm* of the approximate solution $u_h \in S_{h\mathsf{p}} \subset X$ and it measures a violation of (9a). The right-hand side of (24) depends only on u_h and not on u. However, its is impossible to evaluate $\mathcal{R}_h(u_h)$, since the supremum is taken over an infinite-dimensional space. Therefore, in our approach, we seek the maximum over some sufficiently large but finite dimension subspace of X, which is presented in 4.2.

The *second building block* is based on (9b), which characterizes a violation of the conformity of the weak solution and a violation of the Dirichlet boundary condition. It is represented by the value $\mathcal{N}_h(u_h) \geq 0$ given by (8) which we call the *nonconformity* of the approximate solution. In contrast to $\mathcal{R}_h(u_h)$ the quantity $\mathcal{N}_h(u_h)$ is directly computable from (8). Finally, our *error measure* is the sum of squares of the *residuum error* and *nonconformity*, i.e.,

$$\mathcal{E}_h(u_h) := (\mathcal{R}_h(u_h)^2 + \mathcal{N}_h(u_h)^2)^{1/2}. \tag{25}$$

Corollary 1. *Due to Lemma 2.3 we simply observe that* $\mathcal{E}_h(u_h) = 0$ *if and only if* $u_h = u$.

Remark 4.1. *Corollary 1 is essential for the definition of the error measure in the adaptive algorithm. The same property would be valid if the nonconformity is defined by*

$$\mathcal{N}_h(v) := \left(2 \sum_{\Gamma\in\mathscr{F}_h^I} \int_\Gamma h_\Gamma^\alpha [\![v]\!]^2 \,\mathrm{d}S + \sum_{\Gamma\in\mathscr{F}_h^D} \int_\Gamma h_\Gamma^\alpha (v - u_D)^2 \,\mathrm{d}S \right)^{1/2}, \ \alpha \in \mathbb{R}.$$

However, the choice of $\alpha := -1$ *in* (8) *gives the order of convergence* $\mathcal{N}_h(u_h) = O(h^p)$ *if the exact solution is sufficiently regular. The same order of convergence was obtained experimentally for* $\|u - u_h\|_X$ *and* $\rho_h(u_h)$ *given by* (29) *(which approximates* $\mathcal{R}_h(u_h)$*), see Section 6.*

4.2. Global and element residuum estimators

In the previous section, we introduced the error measure $\mathcal{E}_h(u_h) = \sqrt{\mathcal{R}_h(u_h)^2 + \mathcal{N}_h(u_h)^2}$ of the approximate solution $u_h \in S_{hp} \subset X$. Whereas $\mathcal{N}_h(u_h)$ is easy to evaluate, the quantity $\mathcal{R}_h(u_h)$ has to be approximated in a suitable way, which is presented in this section. For each $K \in \mathscr{T}_h$ and each integer $p \geq 0$, we define the space

$$S_K^p \quad := \quad \{\phi_h \in X,\ \phi_h|_K \in P^p(K),\ \phi_h|_{\Omega\setminus K} = 0\}. \tag{26}$$

Obviously, $S_K^p \subset S_K^{p+1} \subset S_K^{p+2} \subset \ldots,\ K \in \mathscr{T}_h$. Moreover, we put

$$S_{hp}^+ := \{\phi \in X; \phi = \sum_{K\in\mathscr{T}_h} c_K\phi_K,\ c_K \in \mathbb{R},\ \phi_K \in S_K^{p_K+1},\ K \in \mathscr{T}_h\}. \tag{27}$$

Finally, we observe that $S_{hp} \subset S_{hp}^+$.

Now, we define the *element residuum estimator*

$$\rho_{h,K}(u_h) := \sup_{0\neq\psi_h\in S_K^{p_K+1}} \frac{\tilde{c}_h(u_h,\psi_h)}{\|\psi_h\|_X} = \sup_{\psi_h\in S_K^{p_K+1},\|\psi_h\|_X=1} \tilde{c}_h(u_h,\psi_h), \qquad u_h \in X, \tag{28}$$

for each $K \in \mathscr{T}_h$ and the *global residuum estimator*

$$\rho_h(u_h) := \sup_{0\neq\psi_h\in S_{hp}^+} \frac{\tilde{c}_h(u_h,\psi_h)}{\|\psi_h\|_X} = \sup_{\psi_h\in S_{hp}^+,\|\psi_h\|_X=1} \tilde{c}_h(u_h,\psi_h), \qquad u_h \in X, \tag{29}$$

which are easily computable quantities if $\|\cdot\|_X$ is suitably chosen, see Section 4.4.

Obviously, if $u \in X$ is the exact solution of (3) then consistency (9a) implies $0 = \rho_h(u) = \rho_{h,K}(u),\ K \in \mathscr{T}_h$. Moreover, we have immediately a lower bound

$$\rho_h(u_h) \leq \mathcal{R}_h(u_h) = \|Au_h - Au\|_{X'}, \tag{30}$$

since ρ_h is the supremum over subspace $S_{hp}^+ \subset X$. However, it is open if there exists an upper bound, i.e., $\mathcal{R}_h(u_h) \leq C\rho_h(u_h)$, where $C > 0$. This will be the subject of further research.

Remark 4.2. *It would be possible to define space S_{hp}^+ in a different way, e.g., to enrich it be polynomials of even higher degree or introduce some interelement splitting of elements $K \in \mathscr{T}_h$. However, any further enrichment of S_{hp}^+ requires additional computational time and the numerical experiments presented at the end of this paper shows that the presented choice of S_{hp}^+ is sufficient.*

Remark 4.3. *Obviously, it is possible to define estimators $\rho_{h,K}(u_h)$ and $\rho_h(u_h)$ directly by* (28) *and* (29) *without the definition of the residuum error in the dual norm by* (24)*. However, the introducing of the dual norm by* (24) *gives link to other works, e.g., [1, 7, 9, 16].*

4.3. Algebraic residuum estimators

Similarly as in the previous section, we define the estimator corresponding to the *algebraic error residuum*. Let $\tilde{u}_h \in S_{hp}$ be an approximation of u_h corresponding to $\tilde{\boldsymbol{U}}_h := \boldsymbol{U}_h^n \in \mathbb{R}^{N_h}$ (= the output of the iterative process (17) – (18)) by (14).

We define the *algebraic residuum estimator*

$$\rho_h^A(\tilde{u}_h) := \sup_{0\neq\psi_h\in S_{hp}} \frac{\tilde{c}_h(\tilde{u}_h,\psi_h)}{\|\psi_h\|_X} = \sup_{\psi_h\in S_{hp},\|\psi_h\|_X=1} \tilde{c}_h(\tilde{u}_h,\psi_h) = \sup_{\psi_h\in S_{hp},\|\psi_h\|_X=1} (\tilde{c}_h(\tilde{u}_h,\psi_h) - \tilde{c}_h(u_h,\psi_h)), \tag{31}$$

which measures the algebraic error (the difference between $\tilde{u}_h$ and u_h). The last inequality in (31) follows from (7). Obviously, if process (17) – (18) converges then $\rho_h^A(\tilde{u}_h) \to 0$ for $n \to \infty$. Moreover, relations (29) and (31) give $\rho_h^A(\tilde{u}_h) \leq \rho_h(\tilde{u}_h)$, since in (29) the supremum is taken over the larger space.

Our interest is to find solution $\tilde{u}_h$ such that $\rho_h(\tilde{u}_h) \leq \omega$, where $\omega > 0$ is a given tolerance. It is clear (cf. [35]) that it makes no sense to carry out too many Newton iterations in (17) – (18) in order to decrease $\rho_h^A(\tilde{u}_h)$ to, e.g., machine precision. It is reasonable to stop the iterative process (17) – (18) if

$$\rho_h^A(\tilde{u}_h) \leq \beta \rho_h(\tilde{u}_h), \tag{32}$$

where $\beta \in (0, 1)$. Numerical experiments presented in Section 6 show that the choice $\beta \approx 0.01$ gives very satisfactory results in the sense that the approximation $\tilde{u}_h$ is not influenced by an algebraic error and the nonlinear problem (16) is not oversolved.

4.4. Choice of the norm $\|\cdot\|_X$

In order to ensure a fast evaluation of estimators ρ_h and ρ_h^A, we need to choose the norm $\|\cdot\|_X$ in a suitable way. Let us present the following lemma.

Lemma 4.4. *Let* $(\!(\cdot,\cdot)\!)_X : X \times X \to \mathbb{R}$ *be a scalar product generating the norm* $\|\cdot\|_X$. *Let* $(\!(\cdot,\cdot)\!)_X$ *satisfy the* element-orthogonality *condition*

$$(\!(\psi_h, \psi_h')\!)_X = 0 \quad \forall \psi_h \in S_K^p \; \forall \psi_h' \in S_{K'}^p, \; K \neq K' \; \forall p \geq 0. \tag{33}$$

Then

$$\rho_h(u_h)^2 = \sum_{K \in \mathscr{T}_h} \rho_{h,K}(u_h)^2, \tag{34}$$

Proof. See Appendix A. □

In order to fulfil the favorable property (34), it is not possible to put

$$(\!(u, v)\!)_X := \sum_{K \in \mathscr{T}_h} \int_K \nabla u \cdot \nabla v \, \mathrm{d}x + \sum_{\Gamma \in \mathscr{F}_h^{ID}} \frac{1}{h_\Gamma} \int_\Gamma [\![u]\!][\![v]\!] \, \mathrm{d}S, \; u, v \in X,$$

which would be natural in virtue of numerical analysis presented, e.g., in [2, 14, 18]. Based on numerical experiments, we employ the scalar product

$$(\!(u, v)\!)_X := \delta (u, v)_{L^2(\Omega)} + \varepsilon \sum_{K \in \mathscr{T}_h} (\nabla u, \nabla v)_{L^2(K)}, \; u, v \in X, \tag{35}$$

where δ and ε are constants reflecting a size of "convection" and "diffusion", for the case of the scalar equation (1a) we put $\delta \approx |\boldsymbol{f}(\cdot)|$ and $\varepsilon \approx |\boldsymbol{K}(\cdot)|$. This scalar product satisfies (33) and the corresponding norm

$$\|\cdot\|_X := \left(\delta \|\cdot\|_{L^2(\Omega)}^2 + \varepsilon |\cdot|_{H^1(\Omega, \mathscr{T}_h)}^2 \right)^{1/2}, \tag{36}$$

is very often used in numerical analysis of singularly perturbed problems with $\delta = 1$, see [42].

Therefore, it rests to evaluate the element residuum estimators $\rho_{h,K}, \; K \in \mathscr{T}_h$. This is a standard task of seeking a constrain extrema over $S_K^{p_K+1}$ with the constraint $\|\psi_h\|_X = 1$. This can be done directly very fast since the dimension of $S_K^{p_K+1}, \; K \in \mathscr{T}_h$ is small, namely $\dim(S_K^{p_K+1}) = (p_k + 2)(p_K + 3)/2$ for dimension $d = 2$. See Appendix B, where the evaluations of $\rho_{h,K}, \; K \in \mathscr{T}_h$ is described in details.

4.5. Residuum-nonconformity estimators

We have already mentioned that the second building block of the error measure is given by nonconformity $\mathcal{N}_h(u_h)$ defined by (8). For the purpose of mesh adaptation, we define its local variant

$$\mathcal{N}_{h,K}(v) := \left(\sum_{\Gamma \in \mathscr{F}_h^I \cap \partial K} \int_\Gamma h_\Gamma^{-1} [\![v]\!]^2 \, \mathrm{d}S + \sum_{\Gamma \in \mathscr{F}_h^D \cap \partial K} \int_\Gamma h_\Gamma^{-1} (v - u_D)^2 \, \mathrm{d}S \right)^{1/2}, \quad v \in H^1(\Omega, \mathscr{T}_h). \tag{37}$$

Obviously, from (8) and (37), we have

$$\mathcal{N}_h(v)^2 = \sum_{K\in\mathscr{T}_h} \mathcal{N}_{h,K}(v)^2. \tag{38}$$

Finally, we define the *local* and *global residuum-nonconformity estimators* of the approximate solution $u_h \in S_{h\mathsf{p}}$ by

$$\eta_{h,K}(u_h) := \left(\rho_{h,K}(u_h)^2 + \mathcal{N}_{h,K}(u_h)^2\right)^{1/2}, \quad K \in \mathscr{T}_h, \tag{39a}$$

$$\text{and} \qquad \eta_h(u_h) := \left(\rho_h(u_h)^2 + \mathcal{N}_h(u_h)^2\right)^{1/2} = \left(\sum_{K\in\mathscr{T}_h} \eta_{h,K}(u_h)^2\right)^{1/2}, \tag{39b}$$

respectively. In virtue of (25), (30) and (39), we expect that the global residuum-nonconformity estimator $\eta_h(u_h)$ approximates the error measure $\mathcal{E}_h(u_h)$. In the following we introduce an adaptation technique which produces a hp-mesh and the corresponding approximate solution such that the estimator $\eta_h(u_h)$ is under a given tolerance.

4.6. Computational costs of the residuum-nonconformity estimator

Before we proceed to the definition of the hp-adaptation process, we discuss the computational costs of the residuum-nonconformity estimator. The evaluation of $\mathcal{N}_h(u_h)$ is quite direct and it is negligible in comparison with, e.g., one Newton step in (17) – (18).

The evaluation of $\rho_h(u_h)$ is described in Appendix B. Its most expensive part is the evaluation of $\tilde{c}_h(u_h, \psi_i)$ for each basis function ψ_i of $S^+_{h\mathsf{p}}$. Let us remind that the setting of one vector $\boldsymbol{F}_h(\boldsymbol{U}_h)$ in the Newton-like process (17) – (18) requires evaluation of $\tilde{c}_h(u_h, \psi_i)$ for each basis function ψ_i of $S_{h\mathsf{p}}$.

Since we use hierarchical basis functions, we evaluate $\tilde{c}_h(u_h, \psi_i)$ only for $\psi_i \in S^+_{h\mathsf{p}} \setminus S_{h\mathsf{p}}$ in addition. For simplicity let $p_K = p \; \forall K \in \mathscr{T}_h$, then we obtain

$$\dim(S^+_{h\mathsf{p}}) = \frac{p+3}{p+1}\dim(S_{h\mathsf{p}}).$$

Therefore, evaluation of $\rho_h(u_h)$ requires $(p+3)/(p+1) - 1$ relatively more computational costs than evaluating $\boldsymbol{F}_h(\boldsymbol{U}_h)$. In the worst case scenario ($p = 1$) this factor is equal to one, for increasing p it tends to zero. Furthermore, an evaluation of $\boldsymbol{F}_h(\boldsymbol{U}_h)$ is obviously significantly cheaper than an evaluation of the flux matrix $\mathbb{C}_h(\boldsymbol{U}_h)$ from (18). Thus we estimate (based on our numerical experiences) that evaluation of the proposed residuum-nonconformity estimator requires between 1% – 10% of additional computational time.

5. *hp*-adaptation process

In this section, we present a new hp-adaptive DG technique for the solution of (7). In Section 4, we defined the element and global residuum-nonconformity estimators $\eta_{h,K}$ and η_h, respectively. We employ the norm $\|\cdot\|_X$ given by (36) which guarantees that equality (34) is valid. Let $\mathscr{T}_h$ be a given mesh and $\tilde{u}_h$ the corresponding approximate solution of (7) outgoing from the iterative method (17) – (18) with (32). As already mentioned, our interest is to find $\tilde{u}_h \in S_{h\mathsf{p}}$ such that

$$\eta_h(\tilde{u}_h) \le \omega, \tag{40}$$

where $\omega > 0$ is a given tolerance. Therefore, we employ the condition

$$\eta_{h,K}(\tilde{u}_h) \le \frac{\omega}{\sqrt{\#\mathscr{T}_h}} \qquad \forall K \in \mathscr{T}_h, \tag{41}$$

where $\#\mathscr{T}_h$ denotes the number of elements of $\mathscr{T}_h$. Obviously, if (41) is satisfied then, due to (39b), condition (40) is valid and the adaptation process stops. Otherwise, we mark for refinement all $K \in \mathscr{T}_h$ violating (41).

Furthermore, all marked elements will be refined either by h- or by p-adaptation, namely, either we split a given mother element K into four daughter elements or we increase the degree of polynomial approximation for a given element. Thus a new mesh $\mathscr{T}_{\hat{h}}$ and a new set $\{\hat{p}_K, K \in \mathscr{T}_{\hat{h}}\}$ are created. We interpolate the old solution on a new mesh and perform the next adaptation step till (40) is valid.

5.1. Regularity indicator

The estimation of the regularity of the solution is an essential key of any *hp*-adaptation strategy. Our approach is based on a measure of inter-element jumps which is the base of the jump indicator from [20] and the shock capturing technique from [26]. See also [37] where the measure of the inter-element jumps is used for the shock detection and limiting with DGM for hyperbolic problems. Numerical analysis [14] carried out for the scalar convection-diffusion equation gives

$$\sum_{K\in\mathscr{T}_h}\int_{\partial K}[\![u_h-u]\!]^2\,\mathrm{d}S=\sum_{K\in\mathscr{T}_h}\int_{\partial K}[\![u_h]\!]^2\,\mathrm{d}S\le C\sum_{K\in\mathscr{T}_h}h_K^{2\mu_K-1}|u|^2_{H^{\mu_K}(K)},\tag{42}$$

where u and u_h are the exact and the approximate solutions, respectively, $C>0$ is a constant independent of h and $\mu_K=\min(p_K+1,s_K)$. Moreover, p_K is the degree of the polynomial approximation and s_K is the integer degree of local regularity of u, i.e., $u|_K\in H^{s_K}(K)$, $K\in\mathscr{T}_h$. The a priori error estimates (42) imply that if the exact solution is sufficiently regular then p-adaptation (increasing of the degree of approximation) yields to a higher decrease of the error. Otherwise, h-adaptation (element splitting) is more efficient.

Furthermore, the numerical experiments indicate that

$$\int_{\partial K}[\![u_h-u]\!]^2\,\mathrm{d}S=\int_{\partial K}[\![u_h]\!]^2\,\mathrm{d}S\approx Ch_K^{2\mu_K-1}|u|^2_{H^{\mu_K}(K)},\ K\in\mathscr{T}_h.\tag{43}$$

Based on relation (43), we propose the *regularity indicator*

$$g_K(u_h):=\frac{\int_{\partial K\cap\Omega}[\![u_h]\!]^2\,\mathrm{d}S}{|K|h_K^{2p_K-3}},\quad K\in\mathscr{T}_h,\tag{44}$$

where $|K|$ is the area of $K\in\mathscr{T}_h$. If $s_K\ge p_K+1$, then

$$g_K(u_h)\approx O\left(\frac{h_K^{2p_K+1}}{h_K^2h_K^{2p_K-3}}\right)=O(h_K^2).\tag{45}$$

On the other hand, if $s_K<p_K+1$, then

$$g_K(u_h)\approx O\left(\frac{h_K^{2s_K-1}}{h_K^2h_K^{2p_K-3}}\right)=O(h_K^{2\delta_K}),\tag{46}$$

where $\delta_K=s_K-p_K<1$. Therefore, from (45) and (46) we have

$$g_K(u_h)\approx O(h_K^{\min(2,2\delta_K)}).\tag{47}$$

We already mentioned that if the exact solution is sufficiently regular then p-adaptation is more efficient. However, there is the following question: *If the exact solution $u\in H^{s_K}(K)$ for $K\in\mathscr{T}_h$ which degree of polynomial approximation $\bar{p}_K$ is the optimal one?* By optimal value we mean that *the degrease of the computational error is the highest possible for the given increase of the number of the degrees of freedom*.

From (42) and (43), we can expect that the optimal degree of polynomial approximation satisfies $p_K+1\approx s_K$ and therefore $\bar{p}_K:=\lfloor s_K-1\rfloor+1$ where symbol $\lfloor a\rfloor$ denotes the integer part of $a\in\mathbb{R}$. However, it is not clear if this value $\bar{p}_K$ is the correct one and moreover, if any optimal value even exists. Nevertheless, based on our computational experiences, we formulate the following:

Proposition 5.1. *Let $K\in\mathscr{T}_h$ and the exact solution satisfies $u\in H^{s_K}(K)$. Then the optimal value of the degree of polynomial approximation on K is given by $\bar{p}_K:=\lfloor s_K+1\rfloor+1$.*

In Section 6, we present several numerical experiments which (at least weakly) support the choice of $\bar{p}_K$ from Proposition 5.1.

Remark 5.2. *Let us note that Proposition 5.1 is in agreement with other results. E.g., in [11, Example 5], the exact solution satisfies* $u \in H^1(\Omega) \setminus H^2(\Omega)$ *and has a singularity in the origin. There, the (adaptively chosen) degree of polynomial approximation around the origin was equal to 3. On the other hand, similar example was treated in [24], there degree of polynomial approximation around the singularity was equal to 4.*

Now, we are ready to finish the proposal of our *hp*-adaptation strategy. Let the optimal value of polynomial approximation $\bar{p}_K$ is given by Proposition 5.1. Then for the optimal value $\delta_K := (s_K - \bar{p}_K)$ we obtain the condition $2\delta_K = 2(s_K - \bar{p}_K) \in (-4, -2]$.

Therefore, we use the following strategy. Let $K \in \mathscr{T}_h$, p_K be the degree of polynomial approximation and let $g_K(u_h)$ be given by (44). Then (in virtue of (47)), we use the following *hp*-refinement strategy.

$$\begin{array}{lll} g_K(u_h) \le h_K^{-2} & \Rightarrow p_K \text{ is smaller than } \bar{p}_K & \Rightarrow \text{p-refinement,} \\ h_K^{-2} < g_K(u_h) \le h_K^{-4} & \Rightarrow p_K \text{ corresponds to } \bar{p}_K & \Rightarrow \text{h-refinement,} \\ h_K^{-4} < g_K(u_h) & \Rightarrow p_K \text{ is larger than } \bar{p}_K & \Rightarrow \text{h-refinement \& p-coarsening.} \end{array} \tag{48}$$

5.2. h- and p-adaptation operations

In this paper we introduce several adaptation operations which are supported by our 2D code.

- *h*-refinement: we split a given mother element K into four daughter elements by connecting centers of its edges. Then hanging nodes could appear in the neighboring elements.
- *p*-refinement: we increase the degree of polynomial approximation for a given element K, i.e., we put $p_K := p_K + 1$.
- *h*-coarsening: we reconstruct a mother element K from four daughter elements, which have arisen in a previous adaptation level.
- *p*-coarsening: we decrease the degree of polynomial approximation for a given element K, i.e., we put $p_K := p_K - 1$.
- *hp*-substitution: if four daughter element are not marked for an additional refinement or coarsening and for each of them $g_K(\tilde{u}_h) \le h_K^{-3}$, we reconstruct the mother element K and increase a degree of polynomial approximation on K simultaneously.

The *h*- and *p*- coarsening are performed if the value of the corresponding element residuum estimator $\eta_{h,K}$ is significantly smaller than the tolerance, in practice, if $\eta_{h,K}(\tilde{u}_h) \le 10^{-2}\omega(\#\mathscr{T}_h)^{-1/2}$. The *hp*-substitution leads to a decrease of N_h and thus it exhibits an efficient tool in situation when some singularity is localized after several adaptation steps.

5.3. hp-DGFE algorithm

The whole adaptation process can be schematically written in the following form.

1. let $\omega > 0$ be a given tolerance,
2. let $\mathscr{T}_h$ be a given mesh and S_{hp} the finite element space,
3. by the iterative method (17) – (18) with the aid of the stopping criterion (32), we obtain $\tilde{u}_h$,
4. we evaluate $\eta_{h,K}(\tilde{u}_h)$, $K \in \mathscr{T}_h$ using (39a), $\eta_h(\tilde{u}_h)$ using (39b) and $g_K(\tilde{u}_h)$, $K \in \mathscr{T}_h$ using (47),
5. if $\eta_h(\tilde{u}_h) \le \omega$ then **we stop the computation**
6. for each $K \in \mathscr{T}_h$, we put $\eta_{\max} := \omega(\#\mathscr{T}_h)^{-1/2}$ and $\eta_{\min} := 10^{-2}\eta_{\max}$
   if $\eta_{h,K}(\tilde{u}_h) > \eta_{\max}$ then
   (a) if $g_K(\tilde{u}_h) \le h_K^{-2}$ then we apply the *p*-refinement on K,
   (b) if $h_K^{-2} < g_K(\tilde{u}_h) \le h_K^{-4}$ then we apply the *h*-refinement on K,
   (c) if $h_K^{-4} < g_K(\tilde{u}_h)$ then we apply the *h*-refinement and *p*-coarsening on K,
   if $\eta_{h,K'}(\tilde{u}_h) < \eta_{\min}$ for all daughter elements of the mother element K then
   (a) we apply *h*-coarsening, i.e., we reconstruct the mother element K,
   (b) if $h_{K'}^{-4} < g_{K'}(\tilde{u}_h)$ then we apply *p*-coarsening on the mother element K',
   if $\eta_{\min} \le \eta_{h,K'}(\tilde{u}_h) \le \eta_{\max}$ for all daughter elements of the mother element K then
   (a) if $g_K(\tilde{u}_h) \le h_K^{-3}$ then we apply *hp*-substitution
7. we construct new mesh $\mathscr{T}_h$ and the space S_{hp}, go to step 3.

6. Numerical experiments

In the previous sections, we introduced and developed the adaptive *hp*-DGFE method. Although its theoretical justification is open, we demonstrate its performance in this section by several numerical examples. Let $\tilde{u}_h$ be the approximate solution resulting from iterative method (17) – (18), i.e., the solution influenced by the algebraic error.

Our goal is to document the following aspects of the *hp*-DGFE method:

(A0) verification of Proposition 5.1,

(A1) the same order of convergence of the estimators $\eta_h(\tilde{u}_h)$, $\rho_h(\tilde{u}_h)$ and $\mathcal{N}_h(\tilde{u}_h)$ with respect to h and its relation with the computational error $\|u - \tilde{u}_h\|_X$, (note that $\eta_h(\tilde{u}_h)^2 = \rho_h(\tilde{u}_h)^2 + \mathcal{N}_h(\tilde{u}_h)^2$),

(A2) the efficiency, accuracy and robustness with respect to the nonlinear convection and diffusion of the *hp*-adaptive algorithm from Section 5.3,

(A3) the performance of the stopping criterion (32) in the iterative process (17) – (18).

By the *efficiency* we mean that the *hp*-adaptation method gives the exponential order of convergence of the computational error with respect to the number of degrees of freedom. By the *accuracy* we mean that the computational error converges with the same order as the residuum error estimates.

The aspects (A0) – (A3) are demonstrated by the following numerical examples:

(E0) Poisson problem with a corner singularity,

(E1) linear convection-diffusion equation with weak boundary layers from [10], [22],

(E2) nonlinear convection-diffusion equation with a corner singularity from [34],

(E3) quasi-linear elliptic problem with a regular analytical solution from [32], see also [31], [41],

(E4) quasi-linear elliptic problem with a corner singularity from [32], see also [47],

(E5) linear convection-diffusion equation with the strong exponential boundary layer.

For these cases, we know the exact solution and therefore we are able to evaluate the computational error. Let us note that the computational error is evaluated with the aid of a numerical quadrature, namely the Dunavant rules for triangles [23], which has the optimal order for the given number of integration nodes.

We carried out two types of computations for examples (E1) – (E5):

(C1) computations on uniform triangular grids with mesh step $h_l = h_0/2^l$, $l = 1, 2, 3$, (h_0 is given) with P_p, $p = 1, \dots, 5$ polynomial approximation. We evaluate the computational error $\|u - \tilde{u}_h\|_X$ given by (36), the nonconformity $\mathcal{N}_h(\tilde{u}_h)$ given by (8) and the error residuum estimator $\rho_h(\tilde{u}_h)$ given by (29). Moreover, we present the corresponding experimental orders of convergence (EOC) with respect to h defined by

$$\mathrm{EOC} = \frac{\log e_{h_{l+1}} - \log e_{h_l}}{\log h_{l+1} - \log h_l}, \qquad l = 0, 1, 2, \dots, \tag{49}$$

where e_h denotes either $\|u - \tilde{u}_h\|_X$ or $\mathcal{N}_h(\tilde{u}_h)$ or $\rho_h(\tilde{u}_h)$.

(C2) *hp*-adaptive algorithm from Section 5.3 starting on mesh with step h_0 and P_1 polynomial approximation. We evaluate again $\|u - \tilde{u}_h\|_X$, $\mathcal{N}_h(\tilde{u}_h)$ and $\rho_h(\tilde{u}_h)$ with the corresponding experimental orders of convergence (EOC) with respect to the number of degrees of freedom N_h defined by

$$\mathrm{EOC} = \frac{\log e_{h_{l+1}} - \log e_{h_l}}{\log(1/\sqrt{N_{h_{l+1}}}) - \log(1/\sqrt{N_{h_l}})}, \qquad l = 1, 2, \dots, \tag{50}$$

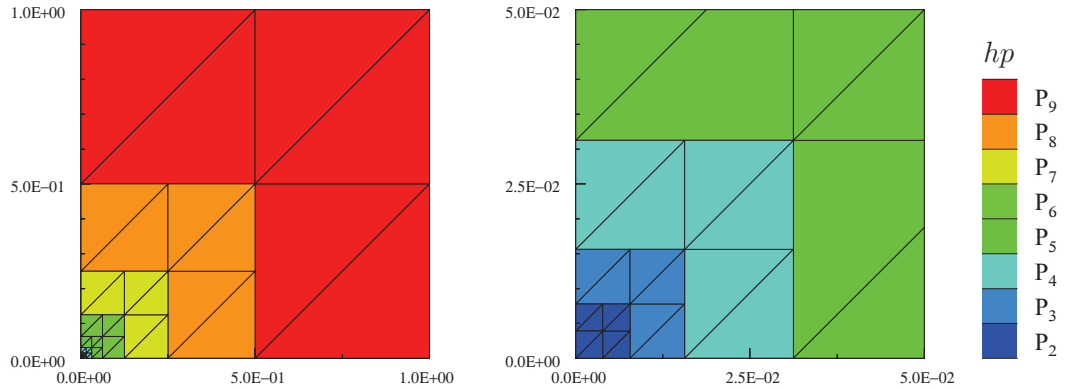

Figure 1: Example (E0): the grid with the corresponding degrees of polynomial approximation obtain by *hp*-refinement (53) after 8 adaptation cycles with $p_* = 2$, the whole domain (left) and its detail (right).

Moreover, for both computations (C1) – (C2) we evaluate the *"effectivity indexes"*

$$i^{\rho}_{\text{eff}} := \frac{\rho_h(\tilde{u}_h)}{\|u - \tilde{u}_h\|_X}, \qquad i^{\eta}_{\text{eff}} := \frac{\eta_h(\tilde{u}_h)}{\left(\|u - \tilde{u}_h\|_X{}^2 + \mathcal{N}_h(\tilde{u}_h)^2\right)^{1/2}} = \frac{\left(\rho_h(\tilde{u}_h)^2 + \mathcal{N}_h(\tilde{u}_h)^2\right)^{1/2}}{\left(\|u - \tilde{u}_h\|_X{}^2 + \mathcal{N}_h(\tilde{u}_h)^2\right)^{1/2}}. \tag{51}$$

Let us note that indexes i^{ρ}_{eff} and i^{η}_{eff} are not standard effectivity indexes since $\rho_h(\tilde{u}_h)$ is the approximation of $\mathcal{R}_h(\tilde{u}_h)$ and not of $\|u - \tilde{u}_h\|_X$. The computations (C1) and (C2) demonstrate aspects (A1) and (A2), respectively. The aspect (A3) is demonstrated for the examples (E2), (E3) and (E4). Finally, for examples (E3) and (E4), we compare the presented *hp*-method with the results from [32] and [31].

6.1. (E0): Poisson problem with a corner singularity

This example serves only for the demonstration of Proposition 5.1. We consider the simple Poisson problem $-\Delta u = f$ with Dirichlet boundary conditions on unit square $(0, 1)^2$, where the exact solution is

$$u(x_1, x_2) = (x_1^2 + x_2^2)^{\alpha/2}, \quad \alpha \in \mathbb{R}. \tag{52}$$

It is possible to show (see [3]) that $u \in H^{\kappa}(\Omega)$, $\kappa \in (0,\ 1 + \alpha)$, where $H^{\kappa}(\Omega)$ denotes the Sobolev-Slobodetskii space of functions with "non-integer derivatives". Therefore, the exact solution has the singularity at the origin $V_0 := [0, 0]$ and it is regular in the rest of the computational domain. We directly employ this a priori knowledge of the regularity of the exact solution and test the following *hp*-adaptation procedure.

We start the computation on a very coarse grid (8 elements arising by the splitting the unit square on four uniform squares and each of them is split on two triangles) with P_1 approximation on each triangle. Moreover, let $p_* \geq 1$ be given. Then in the algorithm from Section 5.3, we skip steps 4. and 5., and the step 6. is replaced by the following *hp*-refinement:

$$\begin{array}{ll} \text{if } (V_0 \text{ is a vertex of } K) \text{ and } (p_K > p_*) & \text{then } h\text{-refinement on } K, \\ & \text{else } p\text{-refinement on } K, \end{array} \qquad K \in \mathcal{T}_h. \tag{53}$$

Figure 1 shows an example of the *hp*-mesh arising from the *hp*-adaptation (53) for $p_* = 2$. We carried out a set of numerical experiments for $\alpha \in \{0.499,\ 0.999,\ 1.499,\ 1.999,\ 2.499,\ 2.999\}$ in (52) with values $p_* \in \{1,\ 2,\ 3,\ 4,\ 5,\ 6\}$ in (53). Figure 2 shows the convergence of the error in the H^1-seminorm with respect to the number of degrees of freedom.

We observe that these results do not give a unique answer which degree of polynomial approximation is the best one for the approximation of the solution with a known regularity. For each tested value α, there exist several values p_* giving almost the identical decrease of the error, the differences are negligible. However, we can conclude that the value $\bar{p}_K$ from Proposition 5.1 belongs among the "good" values p_* for each case.

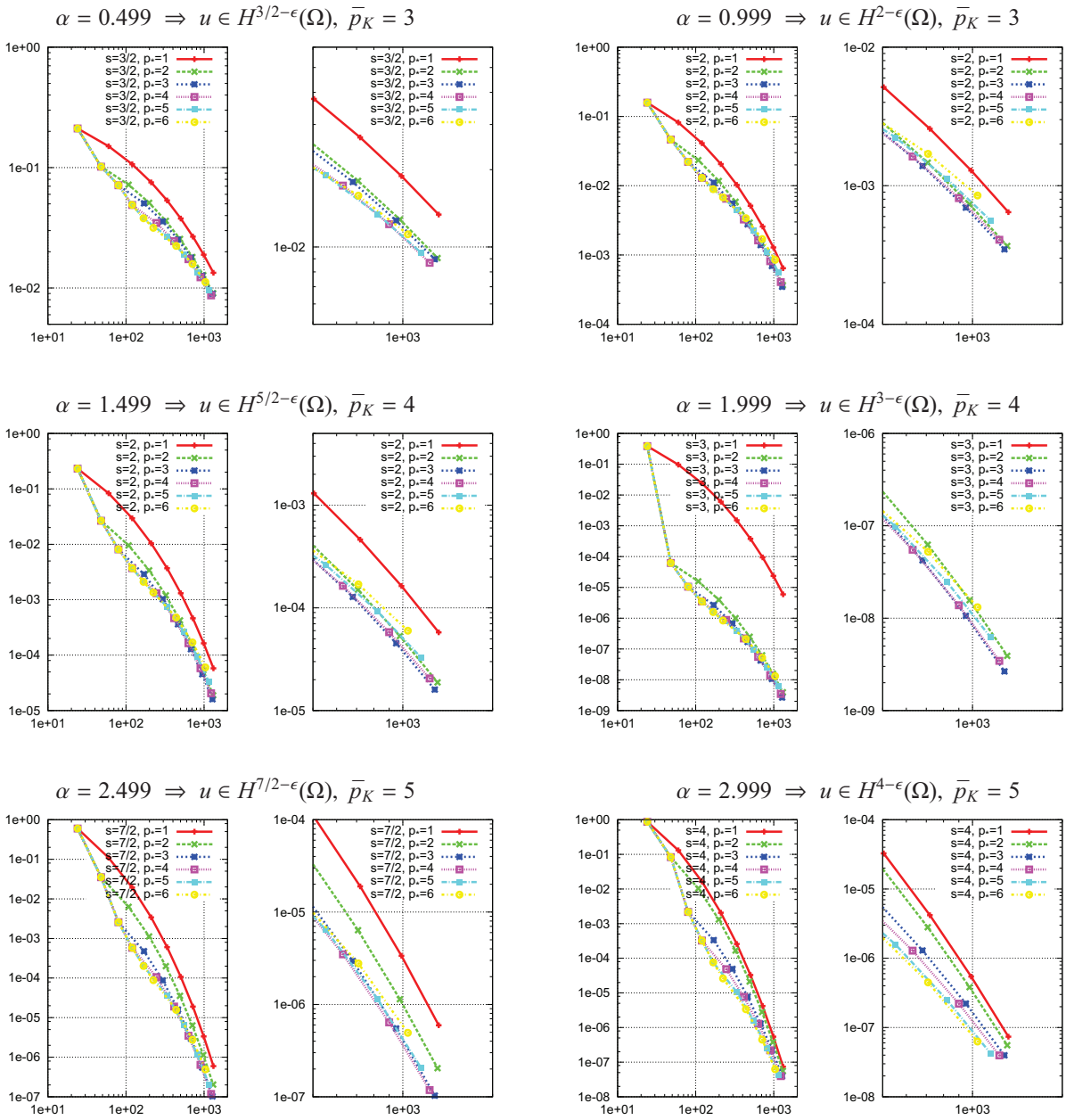

Figure 2: Example (E0), exact solution (52) with $\alpha \in \{0.499,\ 0.999,\ 1.499,\ 1.999,\ 2.499,\ 2.999\}$: convergence of the error in the H^1-seminorm with respect to the number of degrees of freedom for different value of p_* in hp-refinement (53), the whole figure and its detail for each case. For each α, the corresponding regularity of the exact solution ($\epsilon > 0.001$) and the corresponding value of $\bar{p}_K$ from Proposition 5.1 is marked.

(C1) uniform grids

lev	$\#\mathscr{T}_h$	N_h	$\|u-\tilde{u}_h\|_X$	EOC	$\mathcal{N}_h(\tilde{u}_h)$	EOC	$\rho_h(\tilde{u}_h)$	EOC	i^{ρ}_{eff}	i^{η}_{eff}	CPU(s)
1	128	384	3.93E-01	–	1.12E+00	–	1.04E+00	–	2.65	1.29	0.4
1	512	1536	4.44E-01	-0.18	9.59E-01	0.23	8.51E-01	0.29	1.92	1.21	1.0
1	2048	6144	3.62E-01	0.29	6.21E-01	0.63	5.47E-01	0.64	1.51	1.15	3.0
1	8192	24576	2.24E-01	0.69	3.28E-01	0.92	3.01E-01	0.86	1.34	1.12	11.9
2	128	768	3.91E-01	–	8.44E-01	–	6.09E-01	–	1.56	1.12	0.5
2	512	3072	2.59E-01	0.60	5.49E-01	0.62	3.78E-01	0.69	1.46	1.10	1.1
2	2048	12288	1.24E-01	1.06	2.47E-01	1.15	1.66E-01	1.18	1.34	1.08	3.6
2	8192	49152	4.20E-02	1.56	8.21E-02	1.59	5.39E-02	1.63	1.28	1.07	18.8
3	128	1280	2.52E-01	–	5.66E-01	–	3.41E-01	–	1.35	1.07	0.7
3	512	5120	1.12E-01	1.17	2.49E-01	1.19	1.43E-01	1.25	1.28	1.05	1.7
3	2048	20480	3.10E-02	1.85	6.61E-02	1.91	3.77E-02	1.93	1.22	1.04	8.0
3	8192	81920	5.64E-03	2.46	1.14E-02	2.54	6.65E-03	2.50	1.18	1.04	31.2
4	128	1920	1.44E-01	–	3.30E-01	–	1.73E-01	–	1.20	1.03	0.8
4	512	7680	4.07E-02	1.82	9.26E-02	1.83	4.64E-02	1.90	1.14	1.02	2.3
4	2048	30720	6.86E-03	2.57	1.48E-02	2.65	7.31E-03	2.67	1.07	1.01	11.1
4	8192	122880	6.97E-04	3.30	1.45E-03	3.35	7.15E-04	3.35	1.03	1.00	44.1
5	128	2688	7.30E-02	–	1.69E-01	–	7.83E-02	–	1.07	1.01	1.1
5	512	10752	1.40E-02	2.38	3.13E-02	2.43	1.39E-02	2.50	0.99	1.00	3.8
5	2048	43008	1.53E-03	3.20	3.18E-03	3.30	1.40E-03	3.30	0.92	0.99	19.2
5	8192	172032	8.63E-05	4.14	1.74E-04	4.20	7.73E-05	4.18	0.90	0.98	93.0

(C2) hp-adaptation

lev	$\#\mathscr{T}_h$	N_h	$\|u-\tilde{u}_h\|_X$	EOC	$\mathcal{N}_h(\tilde{u}_h)$	EOC	$\rho_h(\tilde{u}_h)$	EOC	i^{ρ}_{eff}	i^{η}_{eff}	CPU(s)
0	128	384	3.93E-01	–	1.12E+00	–	1.04E+00	–	2.65	1.29	0.3
1	128	768	3.91E-01	0.01	8.45E-01	0.82	6.09E-01	1.55	1.56	1.12	0.4
2	128	1248	2.52E-01	1.82	5.67E-01	1.65	3.41E-01	2.40	1.35	1.07	0.7
3	158	1968	1.21E-01	3.23	2.82E-01	3.06	1.63E-01	3.25	1.35	1.06	1.1
4	236	3450	3.72E-02	4.18	8.55E-02	4.26	4.83E-02	4.32	1.30	1.05	1.8
5	380	6322	6.93E-03	5.55	1.50E-02	5.75	7.41E-03	6.19	1.07	1.01	3.6
6	554	10492	7.86E-04	8.60	1.66E-03	8.67	8.40E-04	8.60	1.07	1.01	6.9
7	776	17270	5.73E-05	10.51	1.14E-04	10.76	5.62E-05	10.85	0.98	1.00	12.6
8	938	22438	2.07E-05	7.79	4.28E-05	7.47	2.20E-05	7.15	1.07	1.01	20.2

Table 1: Example (E1) given by (54) – (55) with $\varepsilon = 10^{-2}$: error $\|u-\tilde{u}_h\|_X$, nonconformity $\mathcal{N}_h(\tilde{u}_h)$, residuum error estimate $\rho_h(\tilde{u}_h)$ with the corresponding EOC, indexes i^{ρ}_{eff}, i^{η}_{eff} and the computational time in seconds.

6.2. (E1): Linear convection-diffusion equation with weak boundary layers

We consider the scalar linear convection-diffusion equation (similarly as in [10], [22])

$$-\varepsilon\triangle u - \frac{\partial u}{\partial x_1} - \frac{\partial u}{\partial x_2} = g \quad \text{in } \Omega := (0,1)^2, \tag{54}$$

where $\varepsilon > 0$ is a constant diffusion coefficient. We prescribe a Dirichlet boundary condition on $\partial\Omega$ and the source term g such that the exact solution has the form

$$u(x_1,x_2) = \Big(c_1 + c_2(1-x_1) + e^{-x_1/\varepsilon}\Big)\Big(c_1 + c_2(1-x_2) + e^{-x_2/\varepsilon}\Big) \tag{55}$$

with $c_1 = -e^{-1/\varepsilon}$, $c_2 = -1 - c_1$. The solution contains two boundary layers along $x_1 = 0$ and $x_2 = 0$, whose width is proportional to ε. Here we consider $\varepsilon = 10^{-2}$ and $\varepsilon = 10^{-3}$.

Tables 1 and 2 show the results of computations (C1) and (C2) for problem (54) – (55) with $\varepsilon = 10^{-2}$ and $\varepsilon = 10^{-3}$, respectively, namely the values of the error $\|u-\tilde{u}_h\|_X$, nonconformity $\mathcal{N}_h(\tilde{u}_h)$, residuum error estimate $\rho_h(\tilde{u}_h)$ with the corresponding EOC, indexes i^{ρ}_{eff}, i^{η}_{eff} and the computational times in seconds. We observe from the computations (C1) that all quantities $\|u-\tilde{u}_h\|_X$, $\mathcal{N}_h(\tilde{u}_h)$ and $\rho_h(\tilde{u}_h)$ converge at the similar order of convergence with respect to h. This order is far from the optimal ones ($O(h^p)$) due to a not sufficiently accurate capturing of the boundary layers on coarse grids (relatively to the boundary layer thickness). The optimal values are seen for examples (E2) and (E3). These results demonstrate the aspect (A1).

(C1) uniform grids

lev	$\#\mathcal{T}_h$	N_h	$\|u-\tilde{u}_h\|_X$	EOC	$\mathcal{N}_h(\tilde{u}_h)$	EOC	$\rho_h(\tilde{u}_h)$	EOC	i^{ρ}_{eff}	i^{η}_{eff}	CPU(s)
1	128	384	2.62E-02	–	2.04E+00	–	6.47E-01	–	24.64	1.05	0.5
1	512	1536	5.14E-02	-0.97	2.65E+00	-0.38	8.78E-01	-0.44	17.07	1.05	0.8
1	2048	6144	1.72E-01	-1.74	3.27E+00	-0.30	1.03E+00	-0.23	6.00	1.05	2.4
1	8192	24576	3.47E-01	-1.01	3.66E+00	-0.16	1.09E+00	-0.07	3.13	1.04	9.1
2	128	768	5.15E-01	–	2.02E+00	–	5.28E-01	–	1.02	1.00	0.5
2	512	3072	6.03E-01	-0.23	2.58E+00	-0.35	6.66E-01	-0.34	1.10	1.01	1.2
2	2048	12288	5.39E-01	0.16	3.02E+00	-0.23	7.35E-01	-0.14	1.36	1.01	3.9
2	8192	49152	4.32E-01	0.32	2.97E+00	0.03	6.77E-01	0.12	1.57	1.01	14.7
3	128	1280	9.36E-02	–	2.01E+00	–	4.41E-01	–	4.71	1.02	0.7
3	512	5120	2.91E-01	-1.64	2.50E+00	-0.32	5.38E-01	-0.29	1.85	1.02	1.9
3	2048	20480	3.89E-01	-0.42	2.71E+00	-0.12	5.49E-01	-0.03	1.41	1.01	6.5
3	8192	81920	3.04E-01	0.36	2.19E+00	0.31	4.19E-01	0.39	1.38	1.01	25.1
4	128	1920	5.60E-01	–	1.98E+00	–	3.85E-01	–	0.69	0.98	0.9
4	512	7680	4.85E-01	0.21	2.39E+00	-0.27	4.48E-01	-0.22	0.92	1.00	2.5
4	2048	30720	3.69E-01	0.39	2.32E+00	0.04	4.10E-01	0.13	1.11	1.00	9.1
4	8192	122880	1.96E-01	0.91	1.44E+00	0.69	2.42E-01	0.76	1.23	1.00	35.1
5	128	2688	3.43E-01	–	1.95E+00	–	3.38E-01	–	0.99	1.00	1.2
5	512	10752	4.07E-01	-0.25	2.24E+00	-0.20	3.76E-01	-0.15	0.92	1.00	4.0
5	2048	43008	2.88E-01	0.50	1.88E+00	0.26	2.98E-01	0.34	1.03	1.00	15.3
5	8192	172032	1.12E-01	1.37	8.31E-01	1.18	1.26E-01	1.24	1.13	1.00	71.9

(C2) hp-adaptation

lev	$\#\mathcal{T}_h$	N_h	$\|u-\tilde{u}_h\|_X$	EOC	$\mathcal{N}_h(\tilde{u}_h)$	EOC	$\rho_h(\tilde{u}_h)$	EOC	i^{ρ}_{eff}	i^{η}_{eff}	CPU(s)
0	128	384	2.62E-02	–	2.04E+00	–	6.47E-01	–	24.64	1.05	0.3
1	128	768	5.15E-01	-8.59	2.02E+00	0.02	5.28E-01	0.59	1.02	1.00	0.5
2	146	1076	5.27E-01	-0.13	2.46E+00	-1.15	6.20E-01	-0.95	1.18	1.01	0.7
3	206	1834	4.53E-01	0.57	2.83E+00	-0.53	6.62E-01	-0.25	1.46	1.01	1.0
4	368	4036	3.89E-01	0.39	2.72E+00	0.10	5.46E-01	0.49	1.40	1.01	2.0
5	914	10498	3.04E-01	0.51	2.21E+00	0.43	4.20E-01	0.55	1.38	1.01	3.8
6	1904	22054	1.55E-01	1.81	1.13E+00	1.81	2.10E-01	1.87	1.35	1.01	9.3
7	3746	42724	4.94E-02	3.46	3.44E-01	3.60	6.36E-02	3.60	1.29	1.01	22.8
8	6380	73298	1.00E-02	5.91	6.64E-02	6.09	1.26E-02	6.00	1.26	1.01	45.9
9	7826	103948	1.54E-03	10.74	1.05E-02	10.58	1.98E-03	10.61	1.29	1.01	78.4
10	9725	142471	5.93E-04	6.04	3.87E-03	6.31	7.28E-04	6.33	1.23	1.01	122.7

Table 2: Example (E1) given by (54) – (55) with $\varepsilon = 10^{-3}$: error $\|u-\tilde{u}_h\|_X$, nonconformity $\mathcal{N}_h(\tilde{u}_h)$, residuum error estimate $\rho_h(\tilde{u}_h)$ with the corresponding EOC, indexes i^{ρ}_{eff}, i^{η}_{eff} and the computational time in seconds.

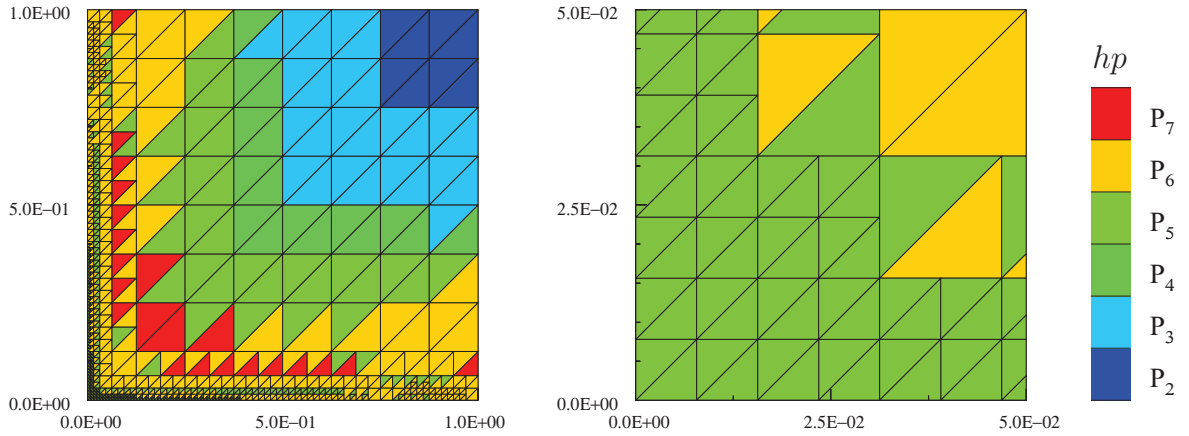

Figure 3: Example (E1) given by (54) – (55) with $\varepsilon = 10^{-2}$: the final grid with the corresponding degrees of polynomial approximation, the whole domain (left) and its detail $(0, 1/20) \times (0, 1/20)$ (right).

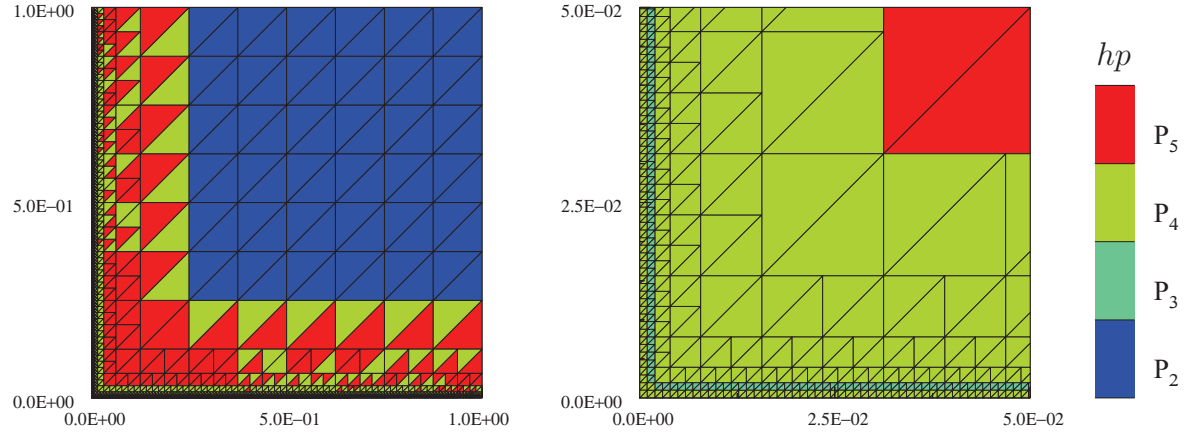

Figure 4: Example (E1) given by (54) – (55) with $\varepsilon = 10^{-3}$: the final grid with the corresponding degrees of polynomial approximation, the whole domain (left) and its detail $(0, 1/20) \times (0, 1/20)$ (right).

Moreover, the computations (C2) show that the presented *hp*-method gives an exponential convergence of error $\|u - \tilde{u}_h\|_X$ with respect to the number of degrees of freedom. The indexes i^{ρ}_{eff}, i^{η}_{eff} are close to one which supports the accuracy of the method. Furthermore, Figures 3 and 4 show the final *hp*-grid obtained with the aid of the *hp*-DGFE algorithm for $\varepsilon = 10^{-2}$ and $\varepsilon = 10^{-3}$, respectively. We observe that the *h*-adaptation was carried out in regions with the boundary layers whereas the *p*-adaptation appears elsewhere. Finally, let us note that the presented strategy is not too efficient for problems with boundary layers since our *h*-adaptation is only isotropic. More efficient is the use of an anisotropic mesh adaptation, e.g., [29].

6.3. (E2): Nonlinear convection-diffusion equation with a corner singularity

We consider the scalar nonlinear convection-diffusion equation

$$-\nabla \cdot (\boldsymbol{K}(u)\nabla u) - \frac{\partial u^2}{\partial x_1} - \frac{\partial u^2}{\partial x_2} = g \quad \text{in } \Omega := (0,1)^2, \tag{56}$$

where $\boldsymbol{K}(u)$ is the nonsymmetric matrix given by

$$\boldsymbol{K}(u) = \varepsilon \begin{pmatrix} 2 + \arctan(u) & (2 - \arctan(u))/4 \\ 0 & (4 + \arctan(u))/2 \end{pmatrix}. \tag{57}$$

The parameter $\varepsilon > 0$ plays a role of an amount of diffusivity and we put $\varepsilon = 10^{-3}$. We prescribe a Dirichlet boundary condition on $\partial\Omega$ and set the source term g such that the exact solution is

$$u(x_1, x_2) = (x_1^2 + x_2^2)^{\alpha/2} x_1 x_2 (1 - x_1)(1 - x_2), \quad \alpha \in \mathbb{R}. \tag{58}$$

We present two choices: $\alpha = 4$ and $\alpha = -3/2$. It is possible to show (see [3]) that $u \in H^{\kappa}(\Omega)$, $\kappa \in (0,\ 3 + \alpha)$. Whereas the choice $\alpha = 4$ gives sufficiently regular solution, the choice $\alpha = -3/2$ leads to the solution with a singularity at $x_1 = x_2 = 0$. Numerical examples presented in [17], carried out for a little different problem, show that this singularity avoids to achieve an order of convergence better than $O(h^{3/2})$ in the L^2-norm and $O(h^{1/2})$ in the H^1-seminorm for any degree of polynomial approximation. Nevertheless, the exact solution is regular outside of the singularity.

Tables 3 and 4 show the results of computations (C1) and (C2) for problem (56) – (58) with $\alpha = 4$ and $\alpha = -3/2$, respectively, namely the values of the error $\|u - \tilde{u}_h\|_X$, nonconformity $\mathcal{N}_h(\tilde{u}_h)$, residuum error estimate $\rho_h(\tilde{u}_h)$ with the corresponding EOC, indexes i^{ρ}_{eff}, i^{η}_{eff} and the computational times in seconds. From the computations (C1), we observe that all quantities $\|u - \tilde{u}_h\|_X$, $\mathcal{N}_h(\tilde{u}_h)$ and $\rho_h(\tilde{u}_h)$ converge at the expected orders $O(h^p)$ for $\alpha = 4$ and $O(h^{1/2})$ for $\alpha = -3/2$. These results demonstrate the aspect (A1).

(C1) uniform grids

lev	$\#\mathscr{T}_h$	N_h	$\|u-\tilde{u}_h\|_X$	EOC	$\mathcal{N}_h(\tilde{u}_h)$	EOC	$\rho_h(\tilde{u}_h)$	EOC	i^{ρ}_{eff}	i^{η}_{eff}	CPU(s)
1	128	384	6.45E-03	–	1.99E-02	–	5.58E-03	–	0.86	0.99	0.7
1	512	1536	1.68E-03	1.94	8.29E-03	1.26	2.81E-03	0.99	1.68	1.03	1.7
1	2048	6144	7.15E-04	1.23	3.81E-03	1.12	1.43E-03	0.98	2.00	1.05	7.8
1	8192	24576	3.45E-04	1.05	1.82E-03	1.06	7.17E-04	0.99	2.08	1.06	52.4
2	128	768	4.42E-04	–	3.01E-03	–	6.35E-04	–	1.44	1.01	0.9
2	512	3072	1.06E-04	2.06	7.61E-04	1.98	1.67E-04	1.92	1.58	1.01	3.2
2	2048	12288	2.56E-05	2.05	1.91E-04	1.99	4.26E-05	1.97	1.67	1.02	18.1
2	8192	49152	6.23E-06	2.04	4.79E-05	2.00	1.07E-05	1.99	1.72	1.02	108.3
3	128	1280	3.87E-05	–	2.75E-04	–	5.22E-05	–	1.35	1.01	1.5
3	512	5120	4.45E-06	3.12	3.32E-05	3.05	6.71E-06	2.96	1.51	1.01	6.4
3	2048	20480	5.41E-07	3.04	4.06E-06	3.03	8.47E-07	2.99	1.56	1.01	35.4
3	8192	81920	6.76E-08	3.00	4.99E-07	3.02	1.06E-07	3.00	1.57	1.01	219.1
4	128	1920	2.75E-06	–	1.73E-05	–	3.05E-06	–	1.11	1.00	2.3
4	512	7680	1.57E-07	4.12	1.04E-06	4.05	1.89E-07	4.01	1.20	1.01	11.8
4	2048	30720	9.50E-09	4.05	6.38E-08	4.03	1.18E-08	4.00	1.24	1.01	62.7
4	8192	122880	5.61E-10	4.08	3.94E-09	4.02	7.42E-10	3.99	1.32	1.01	373.5
5	128	2688	1.10E-07	–	7.04E-07	–	1.13E-07	–	1.02	1.00	4.4
5	512	10752	2.81E-09	5.29	2.11E-08	5.06	3.46E-09	5.03	1.23	1.00	22.6
5	2048	43008	8.14E-11	5.11	6.48E-10	5.02	1.07E-10	5.01	1.32	1.01	115.6
5	8192	172032	1.60E-10	-0.98	1.44E-10	2.17	6.80E-11	0.66	0.42	0.74	708.3

(C2) hp-adaptation

lev	$\#\mathscr{T}_h$	N_h	$\|u-\tilde{u}_h\|_X$	EOC	$\mathcal{N}_h(\tilde{u}_h)$	EOC	$\rho_h(\tilde{u}_h)$	EOC	i^{ρ}_{eff}	i^{η}_{eff}	CPU(s)
0	128	384	6.45E-03	–	1.99E-02	–	5.58E-03	–	0.86	0.99	0.5
1	128	768	4.43E-04	7.73	3.01E-03	5.45	6.35E-04	6.27	1.43	1.01	0.9
2	128	1280	3.87E-05	9.54	2.75E-04	9.36	5.22E-05	9.78	1.35	1.01	1.2
3	128	1920	2.75E-06	13.05	1.73E-05	13.65	3.05E-06	14.02	1.11	1.00	1.8
4	128	2688	1.10E-07	19.12	7.04E-07	19.02	1.13E-07	19.59	1.02	1.00	2.9
5	128	3584	2.49E-09	26.35	1.62E-08	26.24	2.42E-09	26.72	0.97	1.00	4.5
6	128	4608	2.98E-11	35.22	2.23E-10	34.08	3.00E-11	34.92	1.01	1.00	6.8
7	128	5760	3.17E-15	82.03	2.02E-14	83.51	1.56E-14	67.83	4.91	1.25	10.9

Table 3: Example (E2) given by (56) – (58) with $\alpha = 4$: error $\|u-\tilde{u}_h\|_X$, nonconformity $\mathcal{N}_h(\tilde{u}_h)$, residuum error estimate $\rho_h(\tilde{u}_h)$ with the corresponding EOC, indexes i^{ρ}_{eff}, i^{η}_{eff} and the computational time in seconds.

(C1) uniform grids

lev	$\#\mathscr{T}_h$	N_h	$\|u-\tilde{u}_h\|_X$	EOC	$\mathcal{N}_h(\tilde{u}_h)$	EOC	$\rho_h(\tilde{u}_h)$	EOC	i_{eff}^{ρ}	i_{eff}^{η}	CPU(s)
1	128	384	1.32E-02	–	1.41E-01	–	4.52E-02	–	3.43	1.05	0.9
1	512	1536	8.98E-03	0.55	8.21E-02	0.78	2.25E-02	1.00	2.51	1.03	2.0
1	2048	6144	6.36E-03	0.50	5.02E-02	0.71	1.31E-02	0.79	2.06	1.03	6.7
1	8192	24576	4.50E-03	0.50	3.36E-02	0.58	8.55E-03	0.61	1.90	1.02	39.7
2	128	768	5.98E-03	–	6.70E-02	–	1.26E-02	–	2.11	1.01	1.2
2	512	3072	4.19E-03	0.51	4.89E-02	0.45	8.08E-03	0.64	1.93	1.01	3.3
2	2048	12288	2.97E-03	0.50	3.41E-02	0.52	5.34E-03	0.60	1.80	1.01	12.7
2	8192	49152	2.10E-03	0.50	2.38E-02	0.52	3.62E-03	0.56	1.72	1.01	53.7
3	128	1280	5.50E-03	–	6.36E-02	–	6.25E-03	–	1.14	1.00	1.8
3	512	5120	3.84E-03	0.52	4.78E-02	0.41	4.31E-03	0.54	1.12	1.00	5.2
3	2048	20480	2.70E-03	0.51	3.37E-02	0.51	2.91E-03	0.57	1.08	1.00	21.6
3	8192	81920	1.91E-03	0.50	2.37E-02	0.51	1.99E-03	0.55	1.04	1.00	101.5
4	128	1920	4.29E-03	–	5.52E-02	–	4.32E-03	–	1.01	1.00	2.7
4	512	7680	2.97E-03	0.53	3.95E-02	0.48	3.06E-03	0.50	1.03	1.00	7.2
4	2048	30720	2.09E-03	0.51	2.74E-02	0.53	2.02E-03	0.59	0.97	1.00	32.1
4	8192	122880	1.48E-03	0.50	1.92E-02	0.51	1.39E-03	0.55	0.94	1.00	144.2
5	128	2688	4.10E-03	–	4.98E-02	–	3.22E-03	–	0.78	1.00	4.5
5	512	10752	2.82E-03	0.54	3.51E-02	0.51	2.19E-03	0.55	0.78	1.00	13.1
5	2048	43008	1.98E-03	0.51	2.44E-02	0.52	1.45E-03	0.60	0.73	1.00	54.2
5	8192	172032	1.41E-03	0.50	1.72E-02	0.51	1.00E-03	0.54	0.71	1.00	320.5

(C2) hp-adaptation

lev	$\#\mathscr{T}_h$	N_h	$\|u-\tilde{u}_h\|_X$	EOC	$\mathcal{N}_h(\tilde{u}_h)$	EOC	$\rho_h(\tilde{u}_h)$	EOC	i_{eff}^{ρ}	i_{eff}^{η}	CPU(s)
0	128	384	1.32E-02	–	1.41E-01	–	4.52E-02	–	3.43	1.05	0.6
1	128	759	5.98E-03	2.32	6.70E-02	2.18	1.26E-02	3.75	2.11	1.01	1.0
2	128	919	5.50E-03	0.87	6.36E-02	0.55	6.26E-03	7.31	1.14	1.00	1.5
3	128	969	4.30E-03	9.31	5.52E-02	5.35	4.34E-03	13.81	1.01	1.00	1.8
4	134	1089	2.98E-03	6.29	3.96E-02	5.69	3.09E-03	5.86	1.04	1.00	2.2
5	140	1191	2.10E-03	7.81	2.75E-02	8.14	2.07E-03	8.91	0.99	1.00	2.6
6	152	1371	1.49E-03	4.82	1.93E-02	4.99	1.45E-03	5.03	0.97	1.00	2.9
7	158	1456	1.25E-03	5.92	1.62E-02	6.02	1.33E-03	2.95	1.06	1.00	3.3
8	161	1483	9.81E-04	25.21	1.20E-02	30.83	1.06E-03	23.46	1.08	1.00	3.8
9	164	1514	7.11E-04	31.61	8.60E-03	32.64	8.06E-04	26.80	1.13	1.00	4.3
10	170	1584	5.25E-04	13.36	6.24E-03	14.15	6.45E-04	9.85	1.23	1.00	4.8
11	176	1654	4.01E-04	12.42	4.63E-03	13.80	5.47E-04	7.57	1.36	1.00	5.4

Table 4: Example (E2) given by (56) – (58) with $\alpha = -3/2$: error $\|u-\tilde{u}_h\|_X$, nonconformity $\mathcal{N}_h(\tilde{u}_h)$, residuum error estimate $\rho_h(\tilde{u}_h)$ with the corresponding EOC, indexes i_{eff}^{ρ}, i_{eff}^{η} and the computational time in seconds.

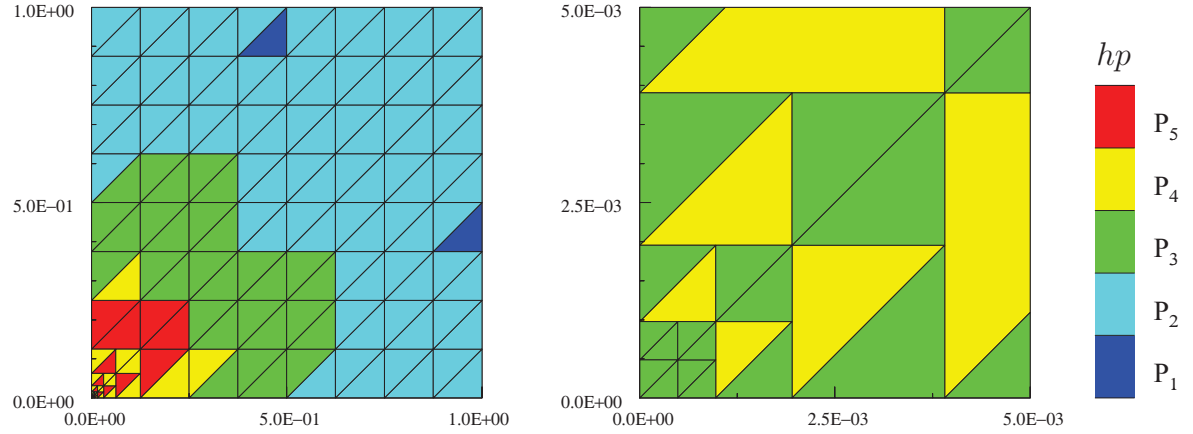

Figure 5: Example (E2) given by (56) – (58) with $\alpha = -3/2$: the final grid with the corresponding degrees of polynomial approximation, the whole domain (left) and its detail $(0, 1/200) \times (0, 1/200)$ (right).

Moreover, the computations (C2) show that the error $\|u - \tilde{u}_h\|_X$ converges exponentially for $\alpha = 4$ and significantly faster than $O(h^{1/2})$ for $\alpha = -3/2$. Furthermore, the indexes i^{ρ}_{eff}, i^{η}_{eff} are close to one. An increase of i^{ρ}_{eff} and i^{η}_{eff} in Table 3 for the last adaptation level is caused by the fact that we are close to the machine accuracy.

Furthermore, Figure 5 shows the final hp-grid obtained with the aid of the hp-DGFE algorithm for $\alpha = -3/2$. (The case $\alpha = 4$ is not interesting since only p-refinement is carried out due to the regularity of the exact solution.) We observe that the h-adaptation was carried out in a small region near the singularity. On the other hand, the p-adaptation appears in regions where the solution is regular.

6.4. (E3): Quasi-linear elliptic problem with a regular solution

We consider the quasi-linear elliptic problem from [32] (see also [31], [41]),

$$-\nabla \cdot (\mu(|\nabla u|)\nabla u) = f \quad \text{in } \Omega := (0, 1)^2, \tag{59}$$

where

$$\mu(|\nabla u|) = 2 + \frac{1}{1 + |\nabla u|}. \tag{60}$$

We consider a homogeneous Dirichlet boundary condition on $\partial\Omega$ and select g such that the analytical solution (59) – (60) is given by

$$u(x_1, x_2) = x_1(1 - x_1)x_2(1 - x_2)(1 - 2x_2)e^{-20(2x_1-1)^2}. \tag{61}$$

Table 5 shows the results of computations (C1) and (C2) for problem (59) – (61), namely the values of the error $\|u - \tilde{u}_h\|_X$, nonconformity $\mathcal{N}_h(\tilde{u}_h)$, residuum error estimate $\rho_h(\tilde{u}_h)$ with the corresponding EOC, indexes i^{ρ}_{eff}, i^{η}_{eff} and the computational times in seconds. From the computations (C1), we observe that all quantities $\|u - \tilde{u}_h\|_X$, $\mathcal{N}_h(\tilde{u}_h)$ and $\rho_h(\tilde{u}_h)$ converge at the expected order $O(h^p)$ since u given by (61) is regular. These results demonstrate the aspect (A1). Similarly as in the previous examples, the computations (C2) show that the computational error $\|u - \tilde{u}_h\|_X$ converges exponentially and the indexes i^{ρ}_{eff}, i^{η}_{eff} are between 1 and 3 and they approach to one for increasing N_h which supports the aspect (A2).

Furthermore, Figure 6, left shows the final hp-grid obtained with the aid of the hp-DGFE algorithm. We observe that the p-adaptation dominates since the exact solution is regular. Our results differ from the results from [32, Example 1], where hp-DGFE computations on quadrilateral grids are performed. Our approach yields to more p-refinements and we achieve the same level of error with a smaller number of degrees of freedom (Table 5), compare with [32, Fig. 1 c,d], where the error 10^{-5} in the $\|\cdot\|_X$-norm was achieved with almost 2E+4 degrees of freedoms.

(C1) uniform grids

lev	$\#\mathcal{T}_h$	N_h	$\|u-\tilde{u}_h\|_X$	EOC	$\mathcal{N}_h(\tilde{u}_h)$	EOC	$\rho_h(\tilde{u}_h)$	EOC	i^{ρ}_{eff}	i^{η}_{eff}	CPU(s)
1	128	384	2.96E-02	–	9.31E-03	–	1.02E-01	–	3.46	3.31	0.5
1	512	1536	1.83E-02	0.70	5.84E-03	0.67	6.83E-02	0.58	3.74	3.57	1.0
1	2048	6144	9.36E-03	0.97	2.85E-03	1.04	3.57E-02	0.93	3.82	3.66	4.0
1	8192	24576	4.71E-03	0.99	1.41E-03	1.02	1.81E-02	0.98	3.84	3.69	18.3
2	128	768	1.19E-02	–	3.84E-03	–	3.85E-02	–	3.23	3.09	0.6
2	512	3072	2.77E-03	2.10	1.20E-03	1.68	9.10E-03	2.08	3.28	3.04	1.7
2	2048	12288	7.11E-04	1.96	3.33E-04	1.85	2.35E-03	1.95	3.31	3.03	7.8
2	8192	49152	1.79E-04	1.99	8.57E-05	1.96	5.94E-04	1.98	3.32	3.02	42.9
3	128	1280	2.00E-03	–	8.07E-04	–	5.33E-03	–	2.67	2.50	0.9
3	512	5120	3.56E-04	2.49	1.50E-04	2.43	1.04E-03	2.36	2.92	2.72	3.2
3	2048	20480	4.57E-05	2.96	1.72E-05	3.12	1.35E-04	2.95	2.96	2.79	15.0
3	8192	81920	5.74E-06	2.99	2.07E-06	3.06	1.70E-05	2.99	2.97	2.81	82.0
4	128	1920	6.62E-04	–	2.13E-04	–	1.78E-03	–	2.69	2.58	1.3
4	512	7680	4.00E-05	4.05	1.72E-05	3.63	1.07E-04	4.06	2.67	2.49	5.2
4	2048	30720	2.56E-06	3.96	1.24E-06	3.79	6.83E-06	3.97	2.67	2.44	24.9
4	8192	122880	1.61E-07	3.99	8.07E-08	3.94	4.31E-07	3.99	2.67	2.43	161.1
5	128	2688	1.00E-04	–	4.50E-05	–	2.35E-04	–	2.35	2.18	2.2
5	512	10752	3.98E-06	4.65	1.79E-06	4.65	9.73E-06	4.60	2.44	2.27	9.9
5	2048	43008	1.28E-07	4.96	5.00E-08	5.16	3.18E-07	4.93	2.48	2.34	58.1
5	8192	172032	4.03E-09	4.99	1.47E-09	5.09	1.01E-08	4.98	2.50	2.37	423.6

(C2) hp-adaptation

lev	$\#\mathcal{T}_h$	N_h	$\|u-\tilde{u}_h\|_X$	EOC	$\mathcal{N}_h(\tilde{u}_h)$	EOC	$\rho_h(\tilde{u}_h)$	EOC	i^{ρ}_{eff}	i^{η}_{eff}	CPU(s)
0	128	384	2.96E-02	–	9.31E-03	–	1.02E-01	–	3.46	3.31	0.4
1	128	768	1.19E-02	2.63	3.84E-03	2.55	3.85E-02	2.82	3.23	3.09	0.7
2	128	1280	2.00E-03	6.99	8.07E-04	6.11	5.33E-03	7.74	2.67	2.50	1.1
3	128	1920	6.62E-04	5.45	2.13E-04	6.56	1.78E-03	5.40	2.69	2.58	1.6
4	128	2688	1.00E-04	11.22	4.50E-05	9.25	2.35E-04	12.04	2.35	2.18	2.6
5	128	3584	2.26E-05	10.36	8.01E-06	12.01	5.10E-05	10.63	2.26	2.16	4.1
6	128	4480	3.42E-06	16.92	1.52E-06	14.89	7.26E-06	17.48	2.12	1.98	6.0
7	128	5416	5.73E-07	18.81	2.24E-07	20.19	1.14E-06	19.46	2.00	1.90	8.3
8	128	6216	1.74E-07	17.34	6.08E-08	18.92	3.36E-07	17.82	1.93	1.85	11.3
9	275	14301	3.73E-08	3.69	7.75E-09	4.94	4.18E-08	5.00	1.12	1.12	21.4

Table 5: Example (E3) given by (59) – (61): error $\|u-\tilde{u}_h\|_X$, nonconformity $\mathcal{N}_h(\tilde{u}_h)$, residuum error estimate $\rho_h(\tilde{u}_h)$ with the corresponding EOC, indexes i^{ρ}_{eff}, i^{η}_{eff} and the computational time in seconds.

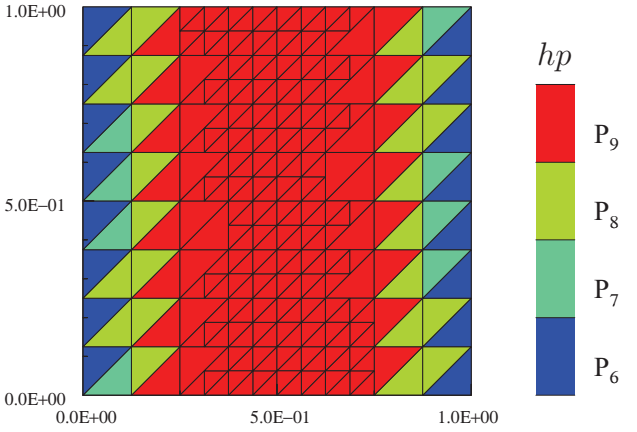

Figure 6: Example (E3) given by (59) – (61): the final grid with the corresponding degrees of polynomial approximation.

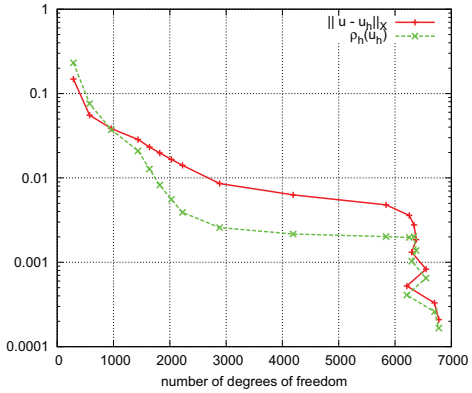

Figure 7: Example (E4) given by (59), (62) – (63): convergence of the error $\|u - \tilde{u}_h\|_X$ and the residuum error estimate $\rho_h(\tilde{u}_h)$ with respect to the number of degrees of freedom.

6.5. (E4): Quasi-linear elliptic problem with a corner singularity

Similarly as in [32] (see also [31], [41]), we consider again the quasi-linear elliptic problem (59) in the L-shaped domain $(-1,1)^2 \setminus [0,1) \times (-1,0)$ with

$$\mu(|\nabla u|) = 1 + e^{-|\nabla u|^2}, \tag{62}$$

with the Dirichlet boundary condition on $\partial\Omega$ and g such that the analytical solution (59), (62) is given by (in polar coordinates)

$$u(r,\varphi) = r^{2/3} \sin(2\varphi/3). \tag{63}$$

We note the $u \notin H^2(\Omega)$ but it is regular outside of $x_1 = x_2 = 0$.

Table 6 shows the results of computations (C1) and (C2) for problem (59), (62) – (63), namely the values of the error $\|u - \tilde{u}_h\|_X$, nonconformity $\mathcal{N}_h(\tilde{u}_h)$, residuum error estimate $\rho_h(\tilde{u}_h)$ with the corresponding EOC, indexes i^{ρ}_{eff}, i^{η}_{eff} and the computational times in seconds. From the computations (C1), we observe that all quantities $\|u - \tilde{u}_h\|_X$, $\mathcal{N}_h(\tilde{u}_h)$ and $\rho_h(\tilde{u}_h)$ converge at the order $O(h^{2/3})$ (we suppose that $u \in H^{\beta}(\Omega)$, $\beta < 1 + 2/3$). These results demonstrate the aspect (A1).

Similarly as in the previous examples, the computations (C2) show that the computational error $\|u - \tilde{u}_h\|_X$ converges exponentially and the indexes i^{ρ}_{eff}, i^{η}_{eff} approach to a constant value (not far from one) for increasing N_h which supports the aspect (A2). In some cases, EOC are negative, since the error as well as the estimate is decreasing even for the decreasing number of degrees of freedom, see Figure 7. It is an advantage our algorithm that it can reduce the number of degrees of freedom as well as the computational error. Finally, Figure 8 shows the final *hp*-grid obtained with the aid of the *hp*-DGFE algorithm. The *h*-adaptation was carried out only in a small region near the singularity.

Table 6 shows that the error level $2 \cdot 10^{-4}$ in the $\|\cdot\|_X$-norm was achieved with about 6800 degrees of freedom. In [31, Figure 3] the same error was achieved with less than 6000 degrees of freedom and in [32, Fig. 2 c,d], with slightly more than 4000 degrees of freedom. From this point of view our approach is a little less efficient than techniques from [31, 32] for problem (59), (62) – (63). However, let us note that techniques from [31, 32] use quadrilateral grids. The number of degrees of freedom for one quadrilateral element is equal to $(p_K + 1)^2$, where p_K is the degree of polynomial approximation in each coordinate direction of a quadrilateral element. On the other hand, the number of degrees of freedom for two triangles (forming one quadrilateral) is equal to $(p_K + 1)(p_k + 2)$. Therefore, triangular elements requires a little more degrees of freedom for the same asymptotic order of convergence. From this point of view the comparison of the efficiency of our approach with results from [31, 32] is not bad.

6.6. (E5): Linear convection-diffusion equation with the strong exponential layer

The exact solution from Section 6.2 contains the boundary layer, however, the diffusive term was relatively large. Therefore, we consider the problem

$$-\varepsilon\triangle u + \frac{\partial u}{\partial x_1} = 1 \quad \text{in } \Omega := (0,1)^2, \tag{64}$$

(C1) uniform grids

lev	$\#\mathcal{T}_h$	N_h	$\|u-\tilde{u}_h\|_X$	EOC	$\mathcal{N}_h(\tilde{u}_h)$	EOC	$\rho_h(\tilde{u}_h)$	EOC	i^{ρ}_{eff}	i^{η}_{eff}	CPU(s)
1	150	450	1.29E-01	–	2.53E-02	–	2.01E-01	–	1.55	1.54	0.7
1	600	1800	8.31E-02	0.64	1.69E-02	0.58	1.31E-01	0.62	1.58	1.56	2.1
1	2400	7200	5.28E-02	0.65	1.12E-02	0.59	8.57E-02	0.61	1.62	1.60	8.0
1	9600	28800	3.35E-02	0.66	7.28E-03	0.63	5.56E-02	0.62	1.66	1.64	36.0
2	150	900	4.79E-02	–	1.46E-02	–	6.58E-02	–	1.37	1.35	1.0
2	600	3600	3.01E-02	0.67	9.46E-03	0.62	4.21E-02	0.65	1.40	1.37	3.6
2	2400	14400	1.89E-02	0.67	6.07E-03	0.64	2.67E-02	0.65	1.42	1.38	12.7
2	9600	57600	1.19E-02	0.67	3.86E-03	0.65	1.69E-02	0.66	1.42	1.39	58.3
3	150	1500	3.33E-02	–	9.73E-03	–	3.21E-02	–	0.96	0.97	1.7
3	600	6000	2.09E-02	0.67	6.20E-03	0.65	2.02E-02	0.67	0.96	0.97	5.3
3	2400	24000	1.32E-02	0.67	3.94E-03	0.65	1.27E-02	0.66	0.97	0.97	21.4
3	9600	96000	8.31E-03	0.67	2.49E-03	0.66	8.04E-03	0.66	0.97	0.97	113.4
4	150	2250	2.45E-02	–	6.82E-03	–	1.79E-02	–	0.73	0.75	2.8
4	600	9000	1.54E-02	0.67	4.32E-03	0.66	1.12E-02	0.69	0.72	0.75	9.2
4	2400	36000	9.73E-03	0.67	2.74E-03	0.66	7.04E-03	0.66	0.72	0.75	34.3
4	9600	144000	6.13E-03	0.67	1.73E-03	0.66	4.45E-03	0.66	0.73	0.75	164.3
5	150	3150	2.00E-02	–	4.99E-03	–	1.09E-02	–	0.54	0.58	4.3
5	600	12600	1.26E-02	0.67	3.15E-03	0.66	6.74E-03	0.69	0.54	0.57	15.3
5	2400	50400	7.93E-03	0.67	2.00E-03	0.66	4.25E-03	0.67	0.54	0.57	58.1
5	9600	201600	5.00E-03	0.67	1.26E-03	0.66	2.69E-03	0.66	0.54	0.58	326.1

(C2) *hp*-adaptation

lev	$\#\mathcal{T}_h$	N_h	$\|u-\tilde{u}_h\|_X$	EOC	$\mathcal{N}_h(\tilde{u}_h)$	EOC	$\rho_h(\tilde{u}_h)$	EOC	i^{ρ}_{eff}	i^{η}_{eff}	CPU(s)
0	96	288	1.49E-01	–	2.89E-02	–	2.32E-01	–	1.56	1.54	0.5
1	96	576	5.56E-02	2.84	1.67E-02	1.58	7.59E-02	3.22	1.37	1.34	1.0
2	96	960	3.86E-02	1.42	1.13E-02	1.54	3.73E-02	2.78	0.97	0.97	2.0
3	96	1435	2.85E-02	1.51	7.92E-03	1.75	2.10E-02	2.87	0.74	0.76	3.3
4	96	1639	2.32E-02	3.09	5.79E-03	4.71	1.27E-02	7.48	0.55	0.59	4.9
5	96	1821	1.98E-02	3.05	4.38E-03	5.31	8.21E-03	8.36	0.42	0.46	6.8
6	96	2027	1.66E-02	3.30	3.41E-03	4.68	5.56E-03	7.28	0.34	0.39	9.0
7	96	2225	1.41E-02	3.46	2.71E-03	4.90	3.90E-03	7.60	0.28	0.33	11.5
8	108	2885	8.59E-03	3.82	1.82E-03	3.09	2.58E-03	3.20	0.30	0.36	15.0
9	138	4191	6.29E-03	1.67	1.39E-03	1.42	2.16E-03	0.94	0.34	0.40	20.0
10	183	5840	4.79E-03	1.64	1.13E-03	1.28	2.02E-03	0.41	0.42	0.47	25.7
11	201	6252	3.59E-03	8.48	9.34E-04	5.50	1.97E-03	0.77	0.55	0.59	31.1
12	216	6337	2.77E-03	41.10	7.96E-04	25.55	2.02E-03	-4.07	0.73	0.75	35.8
13	219	6375	1.86E-03	369.09	5.35E-04	368.53	1.38E-03	349.61	0.74	0.77	41.2
14	228	6297	1.32E-03	-78.54	3.76E-04	-80.13	1.03E-03	-66.89	0.78	0.80	45.7
15	252	6550	8.30E-04	23.70	2.37E-04	23.70	6.49E-04	23.67	0.78	0.80	51.7
16	252	6208	5.23E-04	-16.90	1.49E-04	-16.91	4.10E-04	-16.84	0.78	0.80	57.1
17	282	6700	3.30E-04	12.09	9.43E-05	12.11	2.60E-04	12.02	0.79	0.80	64.0
18	288	6778	2.10E-04	96.63	5.97E-05	96.51	1.66E-04	94.98	0.79	0.81	70.9

Table 6: Example (E4) given by (59), (62) – (63): error $\|u-\tilde{u}_h\|_X$, nonconformity $\mathcal{N}_h(\tilde{u}_h)$, residuum error estimate $\rho_h(\tilde{u}_h)$ with the corresponding EOC, indexes i^{ρ}_{eff}, i^{η}_{eff} and the computational time in seconds.

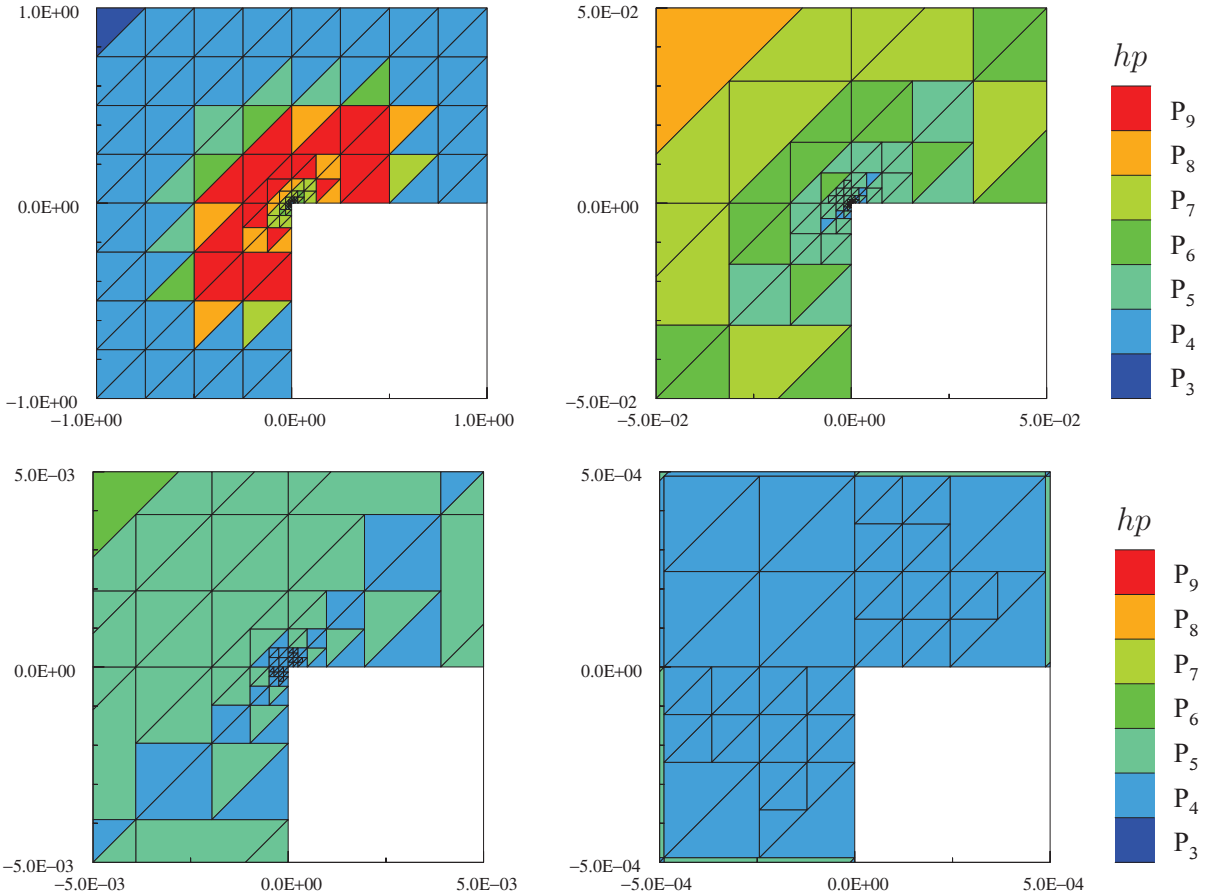

Figure 8: Example (E4) given by (59), (62) – (63): the final grid with the corresponding degrees of polynomial approximation, the whole domain (top left) and its details with magnification 20 (top right), 200 (bottom left) and 2000 (bottom right).

where $0 < \varepsilon \ll 1$ is a constant diffusion coefficient. We employ the values $\varepsilon \in \{10^{-4},\ 10^{-5},\ 10^{-6}\}$. We prescribe the Dirichlet boundary condition on $\partial\Omega$ such that the exact solution has the form

$$u(x_1, x_2) = x_1 - \frac{e^{(x_1-1)/\varepsilon} - e^{-1/\varepsilon}}{1 - e^{-1/\varepsilon}}. \tag{65}$$

The solution possesses a strong exponential boundary layer at $x_1 = 1$, its width is proportional to ε. Therefore, the computations were carried out on a priori refined mesh along the boundary layer, see Figure 10, top left.

Table 7 show the results of computations (C2) for problem (64) – (65), namely the values of the error $\|u - \tilde{u}_h\|_X$, nonconformity $\mathcal{N}_h(\tilde{u}_h)$, residuum error estimate $\rho_h(\tilde{u}_h)$ with the corresponding EOC, indexes i^{ρ}_{eff}, i^{η}_{eff} and the computational times in seconds. Let us recall that $\|u - \tilde{u}_h\|_X$ is evaluated with the aid of the Dunavant quadrature [23] applied to each $K \in \mathscr{T}_h$ and that the Dunavant integration nodes are in the interior of the triangle.

We observe that the computational error $\|u - \tilde{u}_h\|_X$ is small on the initial grid for all ε considered. In the first levels of adaptation, the error increases and after (approximately) 6 – 12 adaptation cycles, the error starts to decrease. However, only for the case $\varepsilon = 10^{-4}$, the adaptation process ends with the smaller error than it has started. For $\varepsilon = 10^{-5}$ and $\varepsilon = 10^{-6}$, the error at the end of the adaptation process is several orders higher than the error on the initial grid. From this point of view, it may seem that the solution on the initial grid is much better than the solution on the adapted grids and hence the mesh adaptation does not makes sense for this case. This effect is explained in the following.

Figure 9 shows the cuts of the approximate solutions along $x_2 = 0.5$ in comparison with the exact solution on the initial mesh (lev = 0) and on the selected meshes obtained by several levels of mesh adaptation (lev = 7 and lev = 12 for $\varepsilon = 10^{-4}$, lev = 10 and lev = 14 for $\varepsilon = 10^{-5}$ and lev = 12 and lev = 17 for $\varepsilon = 10^{-6}$). We found that on the initial mesh (lev = 0), the approximate solution $u_h \approx x_1$, see the first and the second columns in Figure 9. Therefore, the boundary layer is "completely ignored" by the numerical scheme. This is a characteristic property of the discontinuous Galerkin discretization (in contrary to the standard finite element method) since the Dirichlet boundary condition is prescribed by the boundary penalty term

$$\sum_{\Gamma \in \mathscr{F}_h^D} \int_\Gamma \sigma(u - u_D)\, v \,\mathrm{d}S, \qquad \sigma|_\Gamma = \varepsilon\, C_W h_\Gamma^{-1}, \quad h_\Gamma = \operatorname{diam}(\Gamma) \tag{66}$$

in (5). The penalty parameter σ in (66) is small for $\varepsilon \ll 1$ (and for not too small h_Γ). This is a typical example when some physical feature (e.g., the boundary layer) is not captured by the numerical scheme since the characteristic length of the physical feature is many times smaller than the mesh size h.

Hence, if a mesh is not sufficiently refined along $x_1 = 1$ then $u_h \approx x_1$ and thus

$$u - u_h \approx -\frac{e^{(x_1-1)/\varepsilon} - e^{-1/\varepsilon}}{1 - e^{-1/\varepsilon}} =: \tilde{e}_h. \tag{67}$$

Obviously, $\tilde{e}_h(x) = 1$ for all $x = (x_1, x_2) \in \{1\} \times (0, 1)$ and $\tilde{e}_h(x) \ll 1$ for $x = (x_1, x_2) \in (0, 1 - \epsilon) \times (0, 1)$ where $\epsilon \ll 1$ and $\epsilon \sim \varepsilon$. When we evaluate $\|\tilde{e}_h\|_X$ with the aid of the Dunavant quadrature applied to each element of a coarse grid, we obtain a small number, i.e., $\|\tilde{e}_h\|_X \ll 1$. This follows from the fact that the integration nodes on the coarse grid are inside of the set $(0, 1 - \epsilon) \times (0, 1)$ (they are far from the boundary layer) and therefore $\tilde{e}_h(\cdot) \ll 1$ in these integration nodes. Nevertheless, when the mesh is refined near the boundary layer, the new integration nodes arise closer and closer to $x_1 = 1$, $\tilde{e}_h(\cdot)$ in these nodes is bigger and hence the value $\|\tilde{e}_h\|_X$ (computed with the aid of the numerical quadrature mentioned above) increases. This argumentation implies that the values of $\|u - \tilde{u}_h\|_X$ in Table 7 for the lower levels of mesh adaptation are not correct because the quadrature errors are too large. In order to evaluate correct values, it is necessary to employ a better (adaptive) numerical quadrature.

Moreover, whereas the computational error $\|u - \tilde{u}_h\|_X$ as well as the global residuum estimator $\rho_h(\tilde{u}_h)$ on the initial mesh are small, the nonconformity $\mathcal{N}_h(u_h)$ is large due to the second term in (8). Then the proposed adaptive process refines the elements near the wall with $x_1 = 1$. On the refined grids, the penalty parameter $\sigma \sim h_\Gamma^1$ in (66) is higher and thus the boundary penalty is stronger. Therefore, after several levels of mesh adaptations, the boundary layer is captured with an increasing accuracy, see the third and fourth columns of Figure 9. Obviously, in order to achieve the smaller computational error in Table 7 for $\epsilon = 10^{-5}$ and $\epsilon = 10^{-6}$, additional mesh refinement is necessary. However,

(C2) *hp*-adaptation, $\varepsilon = 10^{-4}$

lev	$\#\mathcal{T}_h$	N_h	$\|u-\tilde{u}_h\|_X$	EOC	$\mathcal{N}_h(\tilde{u}_h)$	EOC	$\rho_h(\tilde{u}_h)$	EOC	i^{ρ}_{eff}	i^{η}_{eff}	CPU(s)
0	20	60	6.01E-04	–	1.41E+00	–	4.00E-02	–	66.59	1.00	0.2
1	26	84	1.18E-03	-4.01	1.98E+00	-2.04	6.49E-02	-2.88	55.05	1.00	0.3
2	38	146	2.64E-03	-2.92	2.78E+00	-1.23	9.16E-02	-1.24	34.64	1.00	0.5
3	38	228	5.54E-01	-23.98	2.78E+00	0.00	7.00E-02	1.20	0.13	0.98	1.0
4	68	572	7.55E-01	-0.67	3.87E+00	-0.72	5.79E-02	0.41	0.08	0.98	2.2
5	128	1265	7.55E-01	-0.00	5.29E+00	-0.79	4.16E-02	0.83	0.06	0.99	3.6
6	260	2745	6.88E-01	0.24	6.93E+00	-0.69	8.55E-02	-1.86	0.12	1.00	6.7
7	665	7370	5.85E-01	0.33	8.07E+00	-0.31	1.44E-01	-1.06	0.25	1.00	15.3
8	1601	17040	3.78E-01	1.04	7.03E+00	0.33	1.59E-01	-0.23	0.42	1.00	37.6
9	3254	33597	1.52E-01	2.68	3.65E+00	1.93	9.22E-02	1.61	0.61	1.00	73.4
10	6155	71014	6.10E-02	2.44	1.39E+00	2.57	1.65E-02	4.59	0.27	1.00	142.7
11	12491	142978	1.05E-02	5.02	2.66E-01	4.73	2.78E-03	5.10	0.26	1.00	310.8
12	28631	341645	1.93E-03	3.89	5.06E-02	3.81	3.80E-04	4.57	0.20	1.00	1066.6
13	62303	751569	8.67E-05	7.88	2.43E-03	7.71	4.67E-05	5.32	0.54	1.00	2511.9
14	62795	891916	1.62E-05	19.58	5.17E-04	18.04	1.55E-05	12.85	0.96	1.00	3837.7

(C2) *hp*-adaptation, $\varepsilon = 10^{-5}$

lev	$\#\mathcal{T}_h$	N_h	$\|u-\tilde{u}_h\|_X$	EOC	$\mathcal{N}_h(\tilde{u}_h)$	EOC	$\rho_h(\tilde{u}_h)$	EOC	i^{ρ}_{eff}	i^{η}_{eff}	CPU(s)
0	20	60	5.11E-05	–	1.41E+00	–	6.47E-03	–	126.67	1.00	0.3
1	26	84	7.68E-05	-2.42	2.00E+00	-2.06	1.48E-02	-4.90	192.05	1.00	0.3
2	38	134	1.31E-04	-2.30	2.82E+00	-1.48	2.71E-02	-2.60	205.82	1.00	0.4
3	38	188	1.58E-04	-1.10	2.82E+00	0.00	2.30E-02	0.96	145.26	1.00	0.5
4	68	496	6.40E-03	-7.63	3.99E+00	-0.71	3.46E-02	-0.84	5.40	1.00	0.8
5	128	1111	1.22E-01	-7.32	5.62E+00	-0.85	4.30E-02	-0.54	0.35	1.00	4.1
6	248	2305	4.47E-01	-3.55	7.90E+00	-0.93	3.68E-02	0.43	0.08	1.00	8.1
7	509	5063	7.16E-01	-1.20	1.10E+01	-0.85	6.40E-02	-1.40	0.09	1.00	12.8
8	1199	12122	7.64E-01	-0.15	1.51E+01	-0.73	1.06E-01	-1.17	0.14	1.00	23.3
9	2381	22369	6.97E-01	0.30	2.01E+01	-0.92	1.59E-01	-1.31	0.23	1.00	42.7
10	5288	46699	5.96E-01	0.43	2.43E+01	-0.52	2.07E-01	-0.71	0.35	1.00	86.8
11	12962	116971	4.12E-01	0.80	2.32E+01	0.11	2.10E-01	-0.03	0.51	1.00	203.9
12	30545	278553	1.87E-01	1.83	1.38E+01	1.19	1.30E-01	1.11	0.69	1.00	470.1
13	51005	513038	5.42E-02	4.05	4.16E+00	3.93	3.01E-02	4.78	0.56	1.00	1013.5
14	122522	1223768	7.66E-03	4.50	7.16E-01	4.05	5.22E-03	4.03	0.68	1.00	2619.2

(C2) *hp*-adaptation, $\varepsilon = 10^{-6}$

lev	$\#\mathcal{T}_h$	N_h	$\|u-\tilde{u}_h\|_X$	EOC	$\mathcal{N}_h(\tilde{u}_h)$	EOC	$\rho_h(\tilde{u}_h)$	EOC	i^{ρ}_{eff}	i^{η}_{eff}	CPU(s)
0	20	60	5.01E-06	–	1.41E+00	–	7.08E-04	–	141.23	1.00	0.5
1	26	78	7.13E-06	-2.69	2.00E+00	-2.64	1.94E-03	-7.69	271.87	1.00	0.6
2	38	114	1.04E-05	-1.97	2.83E+00	-1.83	4.92E-03	-4.91	475.06	1.00	0.7
3	38	138	9.29E-06	1.14	2.83E+00	0.00	5.02E-03	-0.20	540.11	1.00	0.9
4	68	300	1.70E-05	-1.56	4.00E+00	-0.89	9.39E-03	-1.61	550.77	1.00	1.2
5	128	701	3.90E-05	-1.95	5.65E+00	-0.82	1.50E-02	-1.10	384.28	1.00	1.8
6	248	1560	1.02E-04	-2.41	7.99E+00	-0.86	2.21E-02	-0.97	216.16	1.00	4.2
7	488	3680	1.34E-03	-6.00	1.13E+01	-0.80	2.66E-02	-0.43	19.79	1.00	31.5
8	968	7736	6.02E-02	-10.23	1.59E+01	-0.93	3.63E-02	-0.84	0.60	1.00	49.8
9	2309	18366	3.31E-01	-3.94	2.24E+01	-0.79	5.62E-02	-1.01	0.17	1.00	86.5
10	4424	35328	6.52E-01	-2.07	3.13E+01	-1.03	8.36E-02	-1.21	0.13	1.00	156.9
11	9032	71963	7.68E-01	-0.46	4.34E+01	-0.91	1.19E-01	-1.00	0.16	1.00	306.8
12	21320	171956	7.20E-01	0.15	5.84E+01	-0.68	1.63E-01	-0.72	0.23	1.00	700.6
13	48776	403909	6.31E-01	0.31	7.36E+01	-0.54	2.08E-01	-0.57	0.33	1.00	1673.4
14	121928	1037468	4.76E-01	0.59	7.72E+01	-0.10	2.25E-01	-0.16	0.47	1.00	4582.0
15	275957	2429960	2.50E-01	1.51	5.44E+01	0.82	1.64E-01	0.75	0.65	1.00	11417.9
16	614204	5445709	8.26E-02	2.75	2.25E+01	2.19	6.67E-02	2.23	0.81	1.00	30659.3
17	1032713	9964991	1.33E-02	6.04	3.84E+00	5.85	9.60E-03	6.42	0.72	1.00	67721.9

Table 7: Example (E5) given by (64) – (65) with $\varepsilon = 10^{-4}$, $\varepsilon = 10^{-5}$ and $\varepsilon = 10^{-6}$: the approximation of the error $\|\overline{u} - \tilde{u}_h\|_X$, nonconformity $\mathcal{N}_h(\tilde{u}_h)$, residuum error estimate $\rho_h(\tilde{u}_h)$ with the corresponding EOC, indexes i^{ρ}_{eff}, i^{η}_{eff} and the computational time in seconds.

a further increase of the number of degrees of freedom is behind of our technical limits. It would be also more efficient to apply an anisotropic mesh adaptation which significantly reduces the number of degrees of freedom for such type of problems. Finally, Figure 10 shows the details of the final *hp*-grids around the boundary layers for each case, a very strong *h*-refinement around the boundary layer is observed.

6.7. Demonstration of aspect (A3) – stopping criterion for the iterative process

Finally, we demonstrate the efficiency of the stopping criterion (32) in the iterative Newton-like method (17) – (18) with $\beta = 10^{-2}$. We denote by $\tilde{u}_h^n,\ n = 0, 1, \dots$ the functions corresponding to the Newton iterations $\boldsymbol{U}_h^n$ by the isomorphism (14). Figure 11 shows the convergence of the Newton approximations $\tilde{u}_h^n$ for each adaptation cycle, particularly the residuum estimator $\rho_h(\tilde{u}_h^n)$ and algebraic residuum estimator $\rho_h^A(\tilde{u}_h^n)$ for examples (E2) (with $\alpha = -3/2$), (E3) and (E4), respectively.

We observe that the iterative processes are stopped at each adaptation cycle when $\rho_h(\tilde{u}_h^n)$ changes only negligibly. We deduce that any additional iteration would decrease $\rho_h^A(\tilde{u}_h^n)$ but not $\rho_h(\tilde{u}_h^n)$. For (E2) and (E3) only few Newton iterations are performed at each adaptation cycle, for (E4) these numbers are higher due the singularity. Finally, this Figure contains also the ℓ^2-norm of the residuum $\boldsymbol{F}_h(\tilde{\boldsymbol{U}}_h)$ for completeness.

7. Conclusion and outlook

In this article, we presented a new *hp*-adaptive method for the solution of convection-diffusion problems. This approach is based on a combination of the residuum nonconformity estimator and the regularity indicator. Numerical experiments show that the presented method gives an exponential order of convergence of the computational error with respect to the number of degrees of freedom and that the residuum nonconformity estimator converges with the same order as the computational error. These properties were observed for problems with a regular solution, a corner singularity and boundary layer, for problems with linear as well as non-linear convection and diffusion. The subject of further research is the numerical analysis of the presented method, an extension to evolution problems and the development of an anisotropic mesh adaptation.

Appendix A. Proof of Lemma 4.4

Proof. Let $u_h \in S_{h\mathsf{p}}$ be the approximate solution. Within this proof, we put $F(\phi_h) := \tilde{c}_h(u_h, \phi_h)$, $\phi_h \in S_{h\mathsf{p}}^+$, F is a linear functional. Moreover, let $\phi_K \in S_K^{p_K+1}$, $K \in \mathscr{T}_h$ denote functions attaining the corresponding local maxima (28), i.e., $\|\phi_K\|_X = 1$ and $\eta_{h,K}(u_h) = F(\phi_K)$, $K \in \mathscr{T}_h$. In order to prove the Lemma, we need to verify that

$$\max_{\phi_h \in S_{h\mathsf{p}}^+, \|\phi_h\|_X = 1} F(\phi_h) = \left(F(\phi_K)^2)\right)^{1/2}. \tag{A.1}$$

Let

$$\psi := \sum_{K \in \mathscr{T}_h} \xi_K \phi_K, \tag{A.2}$$

where $\xi_K \in \mathbb{R}$, $K \in \mathscr{T}_h$ are unknown coefficients. We seek ξ_K, $K \in \mathscr{T}_h$ such that $\|\psi\|_X = 1$ and $F(\psi)$ is maximal. Obviously, due to (33), $1 = \|\psi\|_X^2 = \sum_{K \in \mathscr{T}_h} \xi_K^2$. Moreover,

$$F(\psi) = \sum_{K \in \mathscr{T}_h} \xi_K F(\phi_K) \le \left(\sum_{K \in \mathscr{T}_h} \xi_K^2\right)^{1/2} \left(\sum_{K \in \mathscr{T}_h} F(\phi_K)^2\right)^{1/2} = \left(\sum_{K \in \mathscr{T}_h} F(\phi_K)^2\right)^{1/2}. \tag{A.3}$$

On the other hand, if we put

$$\xi_K := \frac{F(\phi_K)}{\left(\sum_{K \in \mathscr{T}_h} F(\phi_K)^2\right)^{1/2}},\ K \in \mathscr{T}_h \tag{A.4}$$

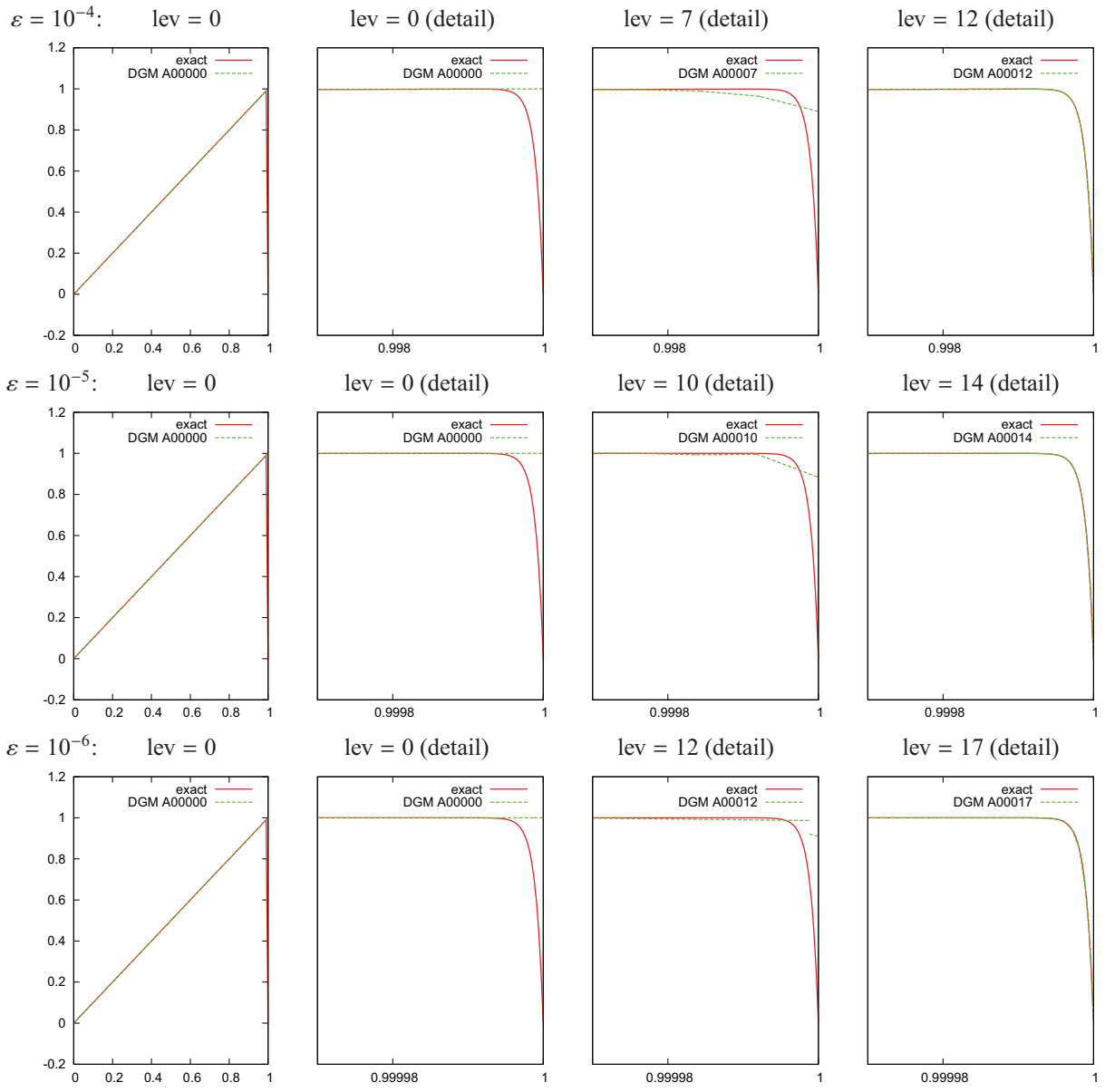

Figure 9: Example (E5) given by (64) – (65): the cut of the approximate solution along $x_2 = 0.5$ in comparison with the exact solution after several adaptation cycles, the cases $\varepsilon = 10^{-4}$ (top), $\varepsilon = 10^{-5}$ (centre) and $\varepsilon = 10^{-6}$ (bottom).

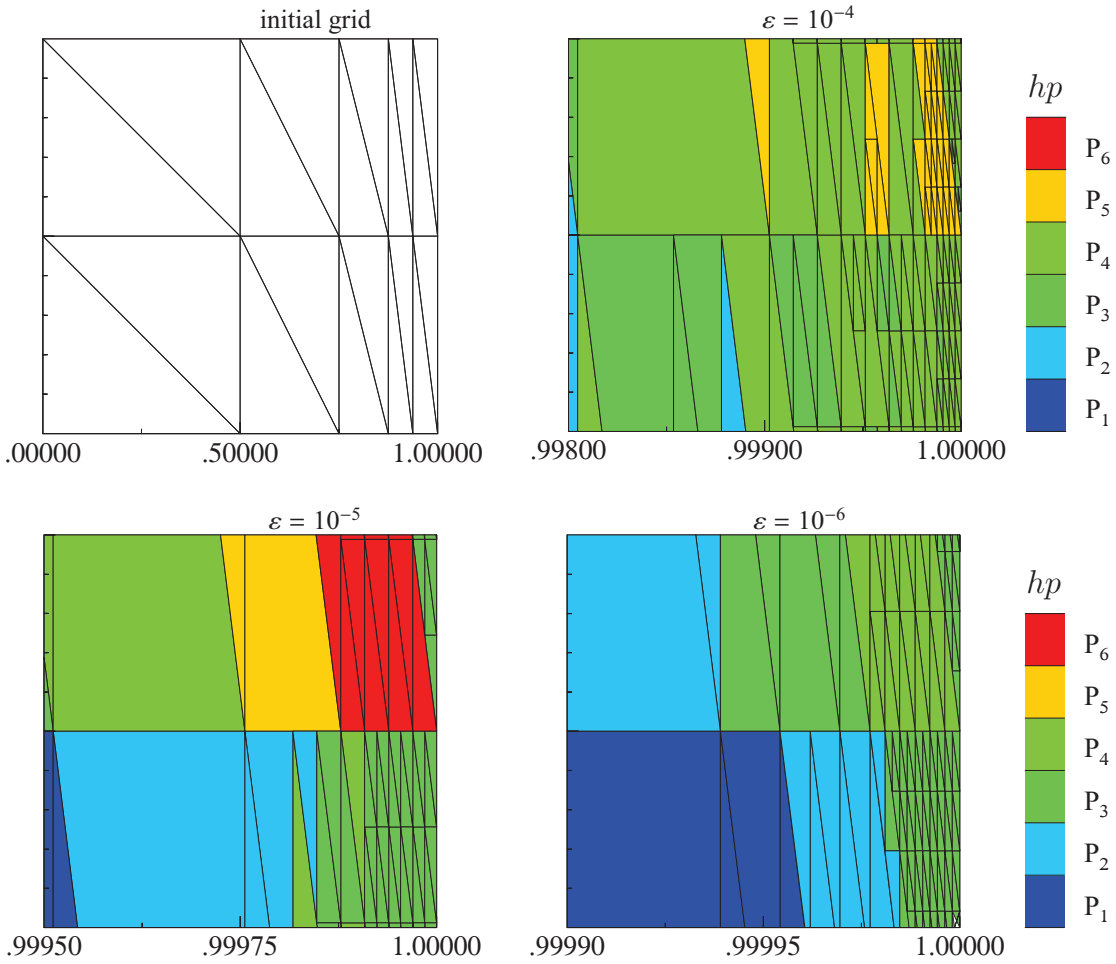

Figure 10: Example (E5) given by (64) – (65): the initial grid and the details of the final grids with the corresponding degrees of polynomial approximation for $\varepsilon = 10^{-4}$, $\varepsilon = 10^{-5}$ and $\varepsilon = 10^{-6}$.

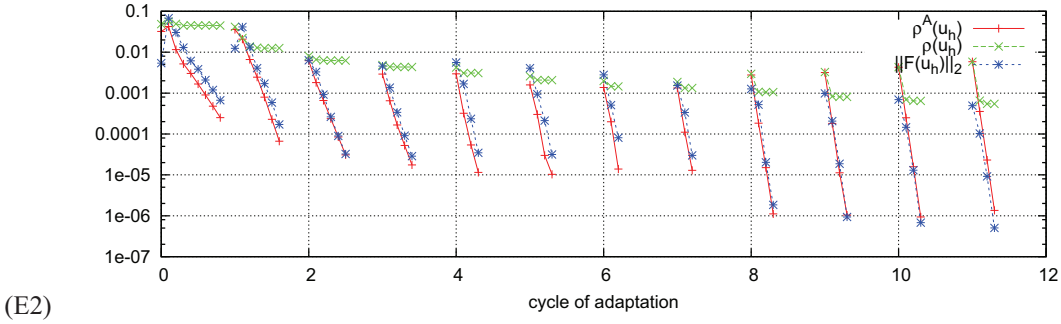

(E2)

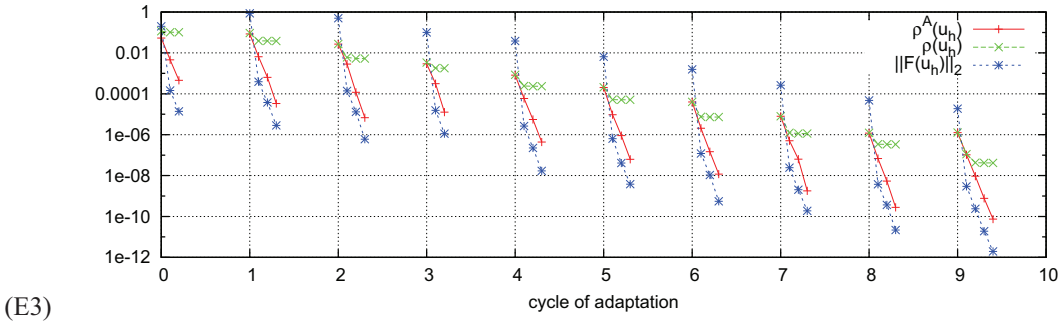

(E3)

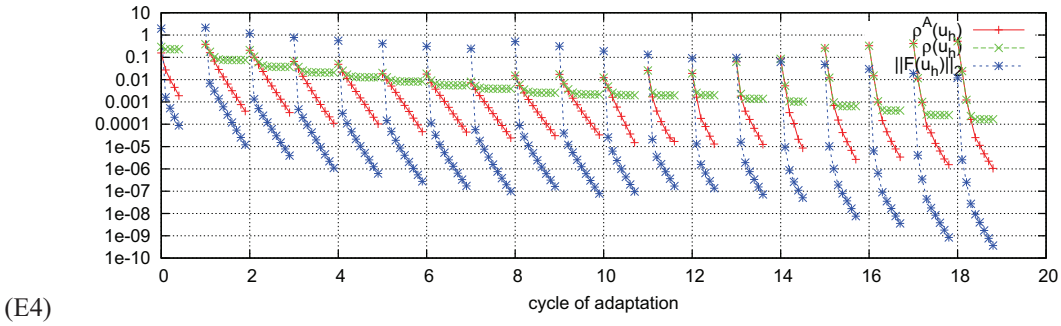

(E4)

Figure 11: Convergence of the Newton approximations $\tilde{u}_h^n$ for each adaptation cycle $l = 0, \ldots, 15$, residuum estimator $\rho_h(\tilde{u}_h^n)$, algebraic residuum estimator $\rho_h^A(\tilde{u}_h^n)$ and the ℓ^2-norm of the algebraic residuum $\boldsymbol{F}_h(\tilde{\boldsymbol{U}}_h)$.

then together with (A.2) we have

$$F(\psi) = \frac{\sum_{K\in\mathcal{T}_h} F(\phi_K)^2}{\left(\sum_{K\in\mathcal{T}_h} F(\phi_K)^2\right)^{1/2}} = \left(\sum_{K\in\mathcal{T}_h} F(\phi_K)^2\right)^{1/2}. \tag{A.5}$$

Hence, the choice (A.4) maximize $F(\psi)$ if ψ is given by (A.2).

Finally, by a contradiction, we prove that $\psi := \sum_{K\in\mathcal{T}_h} \xi_K \phi_K$, with ξ_K, $K \in \mathcal{T}_h$ are given by (A.4), attains the maximum of (29). Let $\psi' := \sum_{K\in\mathcal{T}_h} \xi'_K \phi'_K$, where $\phi'_K \in S_K^{p_K+1}$ and $\xi'_K \in \mathbb{R}$ for all $K \in \mathcal{T}_h$ such that $1 = \|\psi'\|_X^2 = \sum_{K\in\mathcal{T}_h} (\xi'_K)^2$ (due to (33)) and

$$F(\psi') > F(\psi). \tag{A.6}$$

Obviously,

$$F(\psi') = \sum_{K\in\mathcal{T}_h} \xi'_K F(\phi'_K) \le \sum_{K\in\mathcal{T}_h} \xi'_K F(\phi_K) \le \sum_{K\in\mathcal{T}_h} \xi_K F(\phi_K) = F(\psi)$$

which is in contradiction with (A.6). The first inequality follows from the fact that $F(\phi_K) \geq F(\phi'_K),\ K \in \mathscr{T}_h$ and the second inequality (A.3) – (A.5). □

Appendix B. Evaluation of local residuum estimators

We describe how to evaluate

$$\eta_{h,K}(u_h) := \sup_{0 \neq \psi_h \in S_K^{p_K+1}} \frac{\tilde{c}_h(u_h, \psi_h)}{\|\psi_h\|_X}, \quad K \in \mathscr{T}_h, \tag{B.1}$$

given by (28). Let $K \in \mathscr{T}_h$ be an arbitrary but fixed element and $\psi_i,\ i = 1, \ldots, N$ be basis functions of the corresponding space $S_K^{p_K+1}$ given by (26). Let $(\!(\cdot, \cdot)\!)_X$ denote the scalar product which generates the norm $\|\cdot\|_X$. We define the "stiff matrix" $\mathbb{S}$ by

$$\mathbb{S} := \{S_{ij}\}_{i,j=1}^N, \quad S_{ij} := (\!(\psi_i, \psi_j)\!)_X, \quad i, j = 1, \ldots, N. \tag{B.2}$$

Moreover, we put

$$\boldsymbol{d} := \{d_i\}_{i=1}^N, \quad d_i := \tilde{c}_h(u_h, \psi_i), \quad i = 1, \ldots, N. \tag{B.3}$$

Let $\psi \in S_K^{p_K+1}$, then $\psi = \sum_{i=1}^N \xi_i \psi_i$, where $\xi_i \in \mathbb{R},\ i = 1, \ldots, N$ are the basis coefficients. Obviously, $\|\psi\|_X = \sum_{i=1}^N \xi_i \xi_j S_{ij}$. Therefore, the task to find the maximum of (B.1) is equivalent to seek the real coefficients $\xi_i \in \mathbb{R},\ i = 1, \ldots, N$ such that the functional

$$\Psi(\xi_1, \ldots, \xi_N) := \tilde{c}_h(u_h, \psi) = \sum_{i=1}^N \xi_i \tilde{c}_h(u_h, \psi_i) = \sum_{i=1}^N \xi_i d_i \tag{B.4}$$

achieves a maximum provided that $\sum_{i=1}^N \xi_i \xi_j S_{ij} = 1$. This is a standard task of seeking of a constrain extrema which can be solved by the technique of the Lagrange multipliers. Let

$$\overline{\Psi}(\xi_1, \ldots, \xi_N) := \Psi(\xi_1, \ldots, \xi_N) + \lambda \sum_{i=1}^N \xi_i \xi_j S_{ij} = \sum_{i=1}^N \xi_i d_i + \lambda \sum_{i=1}^N \xi_i \xi_j S_{ij}. \tag{B.5}$$

The coefficients $\xi_i,\ i = 1, \ldots, N$ maximizing (B.4) satisfies the relations

$$\begin{aligned} 0 &= \frac{\partial \overline{\Psi}}{\partial \xi_i} = d_i + 2\lambda \xi_i S_{ii} + \lambda \sum_{\substack{j=1 \\ j \neq i}}^N \xi_j S_{ij}, \quad i = 1, \ldots, N, \\ 1 &= \sum_{i=1}^N \xi_i \xi_j S_{ij}. \end{aligned} \tag{B.6}$$

Let $\boldsymbol{\alpha} = (\xi_1, \ldots, \xi_N)^{\mathrm{T}}$. We define a matrix $\overline{\mathbb{S}}$ by

$$\overline{\mathbb{S}} = \{\overline{S}_{ij}\}_{i,j=1}^N, \quad \overline{S}_{ij} = S_{ij} + S_{ii}\delta_{ij}, \tag{B.7}$$

where δ_{ij} is the Kronecker symbol. Then (B.6) can be written in the equivalent form

$$0 = \boldsymbol{d} + \lambda \overline{\mathbb{S}} \boldsymbol{\alpha}, \tag{B.8}$$

$$1 = \boldsymbol{\alpha}^{\mathrm{T}} \mathbb{S} \boldsymbol{\alpha}. \tag{B.9}$$

In virtue of (B.8), we have $\boldsymbol{\alpha} = -\frac{1}{\lambda} \overline{\mathbb{S}}^{-1} \boldsymbol{d}$ and putting into (B.9) we obtain $\lambda^2 := \overline{\boldsymbol{\alpha}}^{\mathrm{T}} \mathbb{S} \overline{\boldsymbol{\alpha}}$, where $\overline{\boldsymbol{\alpha}} := -\overline{\mathbb{S}}^{-1} \boldsymbol{d}$. Finally, we put $\boldsymbol{\alpha} := \overline{\boldsymbol{\alpha}}/\lambda$ and $\eta_{h,K}(u_h) := \sum_{i=1}^N \xi_i d_i$.

The presented approach is very fast, since it is carried out separately for each $K \in \mathscr{T}_h$. Therefore, we have $N = (p_K + 2)(p_K + 3)/2$ for $d = 2$, which is a relatively small number and thus the inversion $\overline{\mathbb{S}}^{-1}$ can be computed directly.

References

[1] L. E. Alaoui, A. Ern, M. Vohralík, Guaranteed and robust a posteriori error estimates and balancing discretization and linearization errors for monotone nonlinear problems, Comput. Methods Appl. Mech. Engrg 200 (2011) 2782–2795.

[2] D. N. Arnold, F. Brezzi, B. Cockburn, L. D. Marini, Unified analysis of discontinuous Galerkin methods for elliptic problems, SIAM J. Numer. Anal. 39 (5) (2002) 1749–1779.

[3] I. Babuška, M. Suri, The *p*- and *hp*- versions of the finite element method. An overview, Comput. Methods Appl. Mech. Eng. 80 (1990) 5–26.

[4] I. Babuška, M. Suri, The *p*− and *hp*−FEM a survey, SIAM Review 36 (1994) 578–632.

[5] F. Bassi, A. Crivellini, S. Rebay, M. Savini, Discontinuous Galerkin solution of the Reynolds averaged Navier-Stokes and k-ω turbulence model equations, Comput. Fluids 34 (2005) 507–540.

[6] F. Bassi, S. Rebay, A high order discontinuous Galerkin method for compressible turbulent flow, in: B. Cockburn, G. E. Karniadakis, C.-W. Shu (eds.), Discontinuous Galerkin Method: Theory, Computations and Applications, Lecture Notes in Computational Science and Engineering 11, Springer-Verlag, 2000, pp. 113–123.

[7] E. Burman, A. Ern, Discontinuous Galerkin approximation with discrete variational principle for the nonlinear Laplacian, Comptes Rendus Mathematique 346 (17-18) (2008) 1013–1016.

[8] C. Carstensen, R. Klose, A posteriori finite element error control for *p*-Laplace problem, SIAM J. Sci. Comput. 25 (3) (2003) 792–814.

[9] A. Chaillou, M. Suri, A posteriori estimation of the linearization error for strongly monotone nonlinear operators, J. Comput. Appl. Math. 205 (1) (2007) 72–87.

[10] C. Clavero, J. L. Gracia, J. C. Jorge, A uniformly convergent alternating direction (HODIE) finite difference scheme for 2D time-dependent convection-diffusion problems, IMA J. Numer. Anal. 26 (2006) 155–172.

[11] L. Demkowicz, W. Rachowicz, P. Devloo, A fully automatic *hp*-adaptivity, J. Sci. Comput. 17 (1-4) (2002) 117–142.

[12] P. Deuflhard, Newton Methods for Nonlinear Problems, vol. 35 of Springer Series in Computational Mathematics, Springer, 2004.

[13] V. Dolejší, On the discontinuous Galerkin method for the numerical solution of the Navier–Stokes equations, Int. J. Numer. Methods Fluids 45 (2004) 1083–1106.

[14] V. Dolejší, Analysis and application of IIPG method to quasilinear nonstationary convection-diffusion problems, J. Comp. Appl. Math. 222 (2008) 251–273.

[15] V. Dolejší, Semi-implicit interior penalty discontinuous Galerkin methods for viscous compressible flows, Commun. Comput. Phys. 4 (2) (2008) 231–274.

[16] V. Dolejší, A. Ern, M. Vohralík, A framework for robust a posteriori error control in unsteady nonlinear advection-diffusion problems, SIAM J. Numer. Anal.Submitted.

[17] V. Dolejší, M. Feistauer, V. Kučera, V. Sobotíková, An optimal $L^\infty(L^2)$-error estimate of the discontinuous Galerkin method for a nonlinear nonstationary convection-diffusion problem, IMA J. Numer. Anal. 28 (3) (2008) 496–521.

[18] V. Dolejší, M. Feistauer, V. Sobotíková, Analysis of the discontinuous Galerkin method for nonlinear convectiondiffusion problems, Comput. Methods Appl. Mech. Eng. 194 (2005) 2709–2733.

[19] V. Dolejší, M. Feistauer, Semi-implicit discontinuous Galerkin finite element method for the numerical solution of inviscid compressible flow, J. Comput. Phys. 198 (2) (2004) 727–746.

[20] V. Dolejší, M. Feistauer, C. Schwab, On some aspects of the discontinuous Galerkin finite element method for conservation laws, Math. Comput. Simul. 61 (2003) 333–346.

[21] V. Dolejší, M. Holík, J. Hozman, Efficient solution strategy for the semi-implicit discontinuous Galerkin discretization of the Navier-Stokes equations, J. Comput. Phys. 230 (2011) 41764200.

[22] V. Dolejší, H.-G. Roos, BDF-FEM for parabolic singularly perturbed problems with exponential layers on layer-adapted meshes in space, Neural Parallel Sci. Comput. 18 (2) (2010) 221–235.

[23] D. A. Dunavant, High degree efficient symmetrical gaussian quadrature rules for the triangle, Int. J. Numer. Methods Eng. 21 (1985) 1129–1148.

[24] T. Eibner, J. M. Melenk, An adaptive strategy for *hp*-FEM based on testing for analyticity, Comput. Mech. 39 (5) (2007) 575–595.

[25] M. Feistauer, J. Felcman, I. Straškraba, Mathematical and Computational Methods for Compressible Flow, Oxford University Press, Oxford, 2003.

[26] M. Feistauer, V. Kučera, On a robust discontinuous Galerkin technique for the solution of compressible flow, J. Comput. Phys. 224 (1) (2007) 208–221.

[27] M. Feistauer, V. Kučera, J. Prokopová, Discontinuous Galerkin solution of compressible flow in time dependent domains, Mathematics and Computers in Simulations 80 (8) (2010) 1612–1623.

[28] G. Gassner, F. Lörcher, C.-D. Munz, A discontinuous Galerkin scheme based on a spacetime expansion. II. viscous flow equations in multi dimensions, J. Sci. Comput. 34 (3) (2008) 260–286.

[29] E. H. Georgoulis, E. Hall, P. Houston, Discontinuous Galerkin methods on *hp*-anisotropic meshes II: A posteriori error analysis and adaptivity, Appl. Numer. Math. 59 (9) (2009) 2179–2194.

[30] R. Hartmann, P. Houston, An optimal order interior penalty discontinuous Galerkin discretization of the compressible Navier–Stokes equations, J. Comput. Phys. 227 (2008) 9670–9685.

[31] P. Houston, D. Schötzau, T. P. Wihler, Energy norm a posteriori error estimation of *hp*-adaptive discontinuous Galerkin methods for elliptic problems, Math. Models Methods Appl. Sci. 17 (33-62).

[32] P. Houston, E. Süli, T. P. Wihler, A posteriori error analysis of *hp*-version discontinuous Galerkin finite element methods for second-order quasilinear elliptic problems, IMA J. Numer. Anal. 28 (2008) 245–273.

[33] P. Houston, E. Sülli, A note on the design of *hp*–adaptive finite element methods for elliptic partial differential equations, Comput. Methods Appl. Mech. Engrg. 194 (2005) 229–243.

[34] J. Hozman, Discontinuous Galerkin method for convection-diffusion problems, Ph.D. thesis, Charles University Prague, Faculty of Mathematics and Physics (2009).

[35] P. Jiránek, Z. Strakoš, M. Vohralík, A posteriori error estimates including algebraic error and stopping criteria for iterative solvers., SIAM J. Sci. Comput. 32 (3) (2010) 15671590.
[36] C. M. Klaij, M. H. van Raalte, H. van der Ven, H. J. W. van der Vegt, *h*-multigrid for space-time discontinuous Galerkin discretizations of the compressible Navier-Stokes equations, J. Comput. Phys. 227 (2007) 1024–1045.
[37] L. Krivodonova, J. Xin, J.-F. Remacle, N. Chevaugeon, J. Flaherty, Shock detection and limiting with discontinuous Galerkin methods for hyperbolic conservation laws, Applied Numerical Mathematics 48 (34) (2004) 323 – 338.
[38] N. Kroll, H. Bieler, H. Deconinck, V. Couallier, H. van der Ven, K. Sorensen (eds.), ADIGMA A European Initiative on the Development of Adaptive Higher-Order Variational Methods for Aerospace Applications, vol. 113 of Notes on Numerical Fluid Mechanics and Multidisciplinary Design, Springer Verlag, 2010.
[39] V. Kučera, Optimal $L^\infty(L^2)$-error estimates for the DG method applied to nonlinear convection-diffusion problems with nonlinear diffusion, Numer. Func. Anal. Optim. 31 (3) (2010) 285–312.
[40] A. Kufner, O. John, S. F. k, Function Spaces, Academia, Prague, 1977.
[41] J. M. Melenk, B. I. Wohlmuth, On residual-based a posteriori error estimation in *hp*-FEM, Adv. Comput. Math. 15 (311-331).
[42] H.-G. Roos, M. Stynes, L. Tobiska, Robust Numerical Methods for Singularly Perturbed Differential Equations. Convection–Diffusion–Reaction and Flow Problems. 2nd ed., Springer-Verlag, Berlin, 2008.
[43] C. Schwab, *p*- and *hp*-Finite Element Methods, Clarendon Press, Oxford, 1998.
[44] P. Šolín, Partial differential equations and the finite element method, Pure and Applied Mathematics, Wiley-Interscience, New York, 2004.
[45] P. Šolín, L. Demkowicz, Goal-oriented *hp*-adaptivity for elliptic problems, Comput. Methods Appl. Mech. Engrg. 193 (2004) 449–468.
[46] M. Vohralík, A posteriori error estimates, stopping criteria and inexpensive implementation, Habilitation thesis, Université Pierre et Marie Curie – Paris 6 (2010).
[47] T. P. Wihler, O. Frauenfelder, C. Schwab, Exponential convergence of the *hp*-DGFEM for diffusion problems, Comput. Math. Appl. 46 (2003) 183–205.